



Theses and Dissertations

2024-08-13

Tools for Planning Multi-Axis Vibration Qualification Tests

Marcus Edward Behling
Brigham Young University

Follow this and additional works at: <https://scholarsarchive.byu.edu/etd>



Part of the [Engineering Commons](#)

BYU ScholarsArchive Citation

Behling, Marcus Edward, "Tools for Planning Multi-Axis Vibration Qualification Tests" (2024). *Theses and Dissertations*. 10533.

<https://scholarsarchive.byu.edu/etd/10533>

This Thesis is brought to you for free and open access by BYU ScholarsArchive. It has been accepted for inclusion in Theses and Dissertations by an authorized administrator of BYU ScholarsArchive. For more information, please contact ellen_amatangelo@byu.edu.

Tools for Planning Multi-Axis Vibration Qualification Tests

Marcus E. Behling

A thesis submitted to the faculty of
Brigham Young University
in partial fulfillment of the requirements for the degree of
Master of Science

Matt Allen, Chair
Jeff Hill
Micah Shepherd
Benjamin Terry

Department of Mechanical Engineering
Brigham Young University

Copyright © 2024 Marcus E. Behling

All Rights Reserved

Tools for Planning Multi-Axis Vibration Qualification Tests

Marcus E. Behling
Department of Mechanical Engineering
Master of Science

BYU Engineering

Abstract

Vibration qualification testing is necessary to ensure that components will endure vibration-induced damage in flight. Multi-axis tests have shown the potential for improvement over single-axis tests, though they require increased planning. This work focuses on planning three critical aspects of these tests: the amount of operational next assembly to include in the test, the size of shakers to use, and the number of shakers to use.

Next assembly selection is studied by varying the amount of next assembly included in the lab test, performing physical tests, and comparing the accuracy of environment reconstruction in each test. In doing so, a tradeoff between impedance, i.e., how well the boundary conditions of the lab test match those of the flight and environment, and controllability, i.e., how many shakers are required to control the lab setup, is revealed. Hence, more next assembly should be included if enough shakers are available to control it, and less next assembly should be included if fewer shakers are available.

The required size of shakers is understood by predicting the required voltage of each shaker before the test. This is first done via dynamic substructuring, though a simplified approach, termed FRF Multiplication, is introduced here. The advantages of this approach are that it is mathematically simpler and does not require drive point FRFs at shaker connection degrees of freedom or even a finite element model (FEM) of the lab setup. It is shown to be a reasonable approximation when the drive point effective mass of the lab setup at each shaker location is much larger than the shaker's armature masses, when the calibration mass is much larger than armature masses, and when the shaker stinger mode is outside of the test frequency band.

Finally, the number of shakers required to give accurate response reconstruction is studied. A modal framework is used to develop theory which is validated through simulated tests. The number of required shakers is found to equal the number of lab setup modes.

Keywords: Vibration Testing, Shaker, Dynamic Substructuring

Acknowledgments

I would like to first thank Matt Allen for his continuous advisement, support in this research, and belief that the project would be a success. I would also like to thank Randy Mayes for helping and sharing his extensive knowledge of the field with me, and Washington DeLima for helping to guide the project as well. I would like to thank the members of the graduate committee, Dr. Hill, Dr. Shepherd, and Dr. Terry, for their insight as well.

I would like to thank my lab mates for their help, particularly Matt Tuman from UW-Madison for helping me get up to speed when I was first starting, and Bradon Thomason for running tests, performing simulations, and helping to write papers.

I would like to thank my family for their continuous support, and particularly my mom for the value for education that she instilled in me growing up.

This work was funded by the Department of Energy's Kansas City National Security Campus, operated by Honeywell Federal Manufacturing & Technologies LLC, under contract number DE-NA0002839, and also by the Utah NASA Space Grant Consortium. I gratefully acknowledge the funding received from both.

Table of Contents

List of Figures vi

List of Tables ix

Nomenclature x

1	Introduction	1
1.1	Problems with Standard Tests	1
1.2	Impedance Matched Multi-Axis Testing	3
1.3	Contributions of Thesis	4
2	Next Assembly Selection	5
2.1	Theory	5
2.2	Experimental Case Study	10
2.3	Conclusions	20
3	Shaker Voltage Prediction	22
3.1	Introduction	22
3.2	MIMO Testing Theory	24
3.3	Shaker Model Calibration	25
3.4	Dynamic Substructuring Theory	31
3.5	FRF Multiplication Theory	34
3.6	FRF Multiplication Case Studies	35
3.7	Results	45
3.8	Uniqueness of Shaker Models	49
3.9	Conclusion	51
4	Number of Shakers	53
4.1	Modal Filtering	53
5	Conclusion	58
	References	61
	Appendices	66
A	Shaker Selection Algorithm	67
B	Shaker Parameter Sensitivity Study	68

List of Figures

- 2.1 Schematic of a traditional environment response reconstruction problem in which measurements are taken on a subcomponent of interest (S) when it is connected to a vehicle (V). In the laboratory, we seek to reconstruct the measured operational environment at a set of measurement points using shakers. 6
- 2.2 Schematic of a TS-IMMAT response reconstruction problem in which a subcomponent of interest (S) is connected to a vehicle (V) through a fixture called a Transmission Simulator (TS). In the laboratory, we seek to reconstruct the measured operational environment using shakers. 7
- 2.3 The instrumented next-level assembly 11
- 2.4 The three assemblies tested are Configuration A with the stool and plate, Configuration B with the stool, plate, and IFP, and Configuration C with the stool, plate, IFP, pillars, and bulkhead 11
- 2.5 Reconstruction ASDs of the controlled accelerometers on the plate (cyan) along with the control ASDs (black) for Configuration C 13
- 2.6 Measured ASDs of the uncontrolled accelerometers on the stool (cyan) along with the environment ASDs (black) for Configuration C 13
- 2.7 Composite of the Frequency Response Functions measured on each of the configurations: (yellow) Configuration A, (red) Configuration B, (blue) Configuration C 14
- 2.8 2nd Fixed Plate Mode of Configuration C, 451 Hz 16
- 2.9 Test Setup on Configuration C with Shakers Attached to Interface Plate 17
- 2.10 Photo of test setup for Configuration B-2 with three shakers in the launch direction and all others removed. 18
- 2.11 Response of the stool on plate system in the launch direction, with Plate accelerometers (CH3, CH6 and CH9) and Stool accelerometers (CH10, CH13 and CH16) 19
- 2.12 Measured ASDs of the plate (left) and the stool (right) from Configuration A-2, the case study where there is a near perfect impedance match between lab and the true environment. 20

- 3.1 Six Shaker MIMO Test Setup (Left) and Schematic Representing Shaker Locations (Right), where the red dots represent Q-Sources on the bottom side of the plate forcing in the launch direction, the yellow arrow represents the LDS shaker forcing in the spin / radial direction, and the blue arrow represents the MS shakers forcing in the radial directions 24
- 3.2 Accelerometer Locations on DUT (Orange) and Next Assembly (Red) 24
- 3.3 Shaker Body (Red), Armature (Orange), and Calibration Mass (Blue) 26
- 3.4 Electrodynamic Shaker Model. Left: Electrical Elements. Right: Mechanical Elements. 26
- 3.5 Calibration Test Setups for MS (Left), LDS (Center), and Q-Source Shakers (Right) 27
- 3.6 Experimental (Red) and Analytical (Blue) Acceleration/Voltage FRFs for MS Shakers 30
- 3.7 Experimental (Red) and Analytical (Blue) Acceleration/Voltage FRFs for LDS Shaker 31
- 3.8 Experimental (Red) and Analytical (Blue) Acceleration/Voltage FRFs for Q-Source Shakers 31
- 3.9 Calibration Setup for Case Study 36
- 3.10 DUT for Case Study 36
- 3.11 Qualification Setup for Case Study 36
- 3.12 Flight Setup for Case Study 37
- 3.13 Simulated Environments for 0.1 kg DUT (Blue) and 25 kg DUT (Green) 37
- 3.14 Force Auto Spectra: Truth (Black) and Estimate Obtained Using FRF Multiplication (Blue) 38
- 3.15 Stinger Force/Armature Force FRF for Calibration (Black) and Qualification (Red) Systems with $m_{DUT} = 0.1$ kg and $m_{DUT} = 25$ kg. $\omega_{n,cal} = \omega_{n,DUT}$ 39
- 3.16 Stinger Force/Armature Force FRF for Calibration (Black) and Qualification (Red) Systems with $m_{DUT} = 0.1$ kg and $m_{DUT} = 25$ kg. $\omega_{n,DUT} = 0.5\omega_{n,cal}$ 40
- 3.17 Stinger Force / Armature Force FRF for Calibration (Black) and Qualification (Red) Systems with $m_{DUT} = 0.1$ kg and $m_{DUT} = 25$. $f_{n,cal}=25,200$ Hz.(Note the reduced vertical scale relative to the prior figures.) 40
- 3.18 Free-Free Bending Mode of DUT, 795 Hz, with Fixture Attachment Location in Red and Stool Attachment Location in Yellow 43
- 3.19 Stinger Force/Voltage FRF in Calibrated Shaker Model (Blue) and Substructured Qualification Setup with Shaker Attached to Interface Plate (Red) and Top of Stool (Black) 44
- 3.20 Summary of Conditions for Success of FRF Multiplication 44

- 3.21 Stool Accelerometer PSDs in Launch, Spin, and Radial Directions at Three Locations in the Flight Environment (Black) and MIMO Test (Green), with predictions from Substructuring (Blue), FEM Multiplication (Red), and Roving Hammer Multiplication (Cyan) 46
- 3.22 Voltage PSDs for MIMO Test (Green), Substructuring (Blue), FRF Multiplication with FEM (Red), and FRF Multiplication with Roving Hammer Measurements (Cyan) 47
- 3.23 Measured (Red) and Model (Blue) Acceleration/Voltage FRFs for First and Second Parameter Sets for the MS Shaker 49
- 3.24 MS Electrical Impedance FRFs for Parameter Set 1 (Black) and Parameter Set 2 (Blue) 51

- 4.1 First (783 Hz) and Third (885 Hz) Free-Free Mode Shapes of DUT 54
- 4.2 Original Flight Environment (Black) Compared to Environment Reconstructed Using First 9 FEM Modes (Cyan) 54
- 4.3 Elastic Environment (Black) and Simulated Reconstruction (Cyan) with Three Shakers 56
- 4.4 Lab Modal Responses in 3 Shaker Simplified Environment Test (Red) and 6 Shaker Unmodified Environment Test (Blue) 57

- B.1 Analytical Acceleration/Voltage FRF with Nominal Stinger Damping Value (Black) and 3x Nominal Value (Red) 68
- B.2 Analytical Acceleration/Voltage FRF with Nominal Flexure Damping Value (Black) and 50x Nominal Value (Red) 69
- B.3 Analytical Acceleration/Voltage FRF with Nominal Resistance Value (Black) and 3x Nominal Value (Red) 69
- B.4 Analytical Acceleration/Voltage FRF with Nominal Inductance Value (Black) and 3x Nominal Value (Red) 69
- B.5 Analytical Acceleration/Voltage FRF with Nominal Back-EMF Constant (Black) and 3x Nominal Value (Red) 70

List of Tables

- 2.1 Error in experimental reconstruction for three assemblies tested 14
- 2.2 Average Shaker RMS Voltage in Tests Performed on Each Configuration 15
- 2.3 RMS dB Error on Configuration C when Shakers are attached to Bulkhead Plate and Interface Plate 17

- 3.1 Parameters Obtained for Each Shaker in the Calibration Process 30
- 3.2 Case Study Parameter Values 36
- 3.3 RMS Force (N) Estimates for Simulated Case Study Tests 38
- 3.4 Shaker RMS Force Limits and Amplifier RMS Output Voltage Limits 45
- 3.5 RMS Shaker Voltage in MIMO Test, Substructured FRF Simulation, and FRF Multiplication Simulations from 100-2000 Hz 48
- 3.6 Two Sets of Parameters Obtained in Calibration for the MS Shaker 50
- 3.7 MIMO Test Simulation with Two Sets of Calibrated Parameters 50

Nomenclature

\square	Matrix
η	Primal Formulation Displacement
Φ	Mode Shape Matrix
\mathbf{B}	Compatibility Matrix
\mathbf{C}	Damping Matrix
\mathbf{K}	Stiffness Matrix
\mathbf{L}	Force Equilibrium Matrix
\mathbf{M}	Mass Matrix
\mathbf{S}	Acceleration Power Spectral Density
ω	Angular Frequency
ω_n	Natural Frequency
$\omega_{0,qual}$	Qualification Setup Anti-Resonance
$\omega_{n,cal}$	Calibration Setup Natural Frequency
$\omega_{n,DUT}$	DUT Natural Frequency
ϕ	Mode Shape Vector
\mathbf{H}	Frequency Response Function
$\{ \}$	Vector
*	Conjugate Transpose
+	Pseudo Inverse
\cdot	Time Derivative
$\ddot{}$	Double Time Derivative
BL	Back-EMF Constant
c_{flex}	Flexure Damping
c_{sting}	Shaker Body Mass
E	Expected Value
E	Shaker Voltage
e	Error
EST	Estimated
F	Physical Force

f	Frequency
g	Interface Force
I	Shaker Current
k_{flex}	Flexure Stiffness
k_{sting}	Stinger Stiffness
L_a	Armature Coil Inductance
m_{arm}	Armature Mass
m_{body}	Shaker Body Mass
m_{cal}	Calibration Mass
m_{DUT}	DUT Mass
$null$	Null Space Operator
Q	Modal Acceleration
R_a	Armature Coil Resistance
RMS	Root-Mean-Square
S	Stool
Sh	Shaker
TS	Transmission Simulator
u	Physical Displacement
V	Vehicle
V	Voltage Input to Amplifier
X	Physical Acceleration
x_{arm}	Armature Displacement
x_{body}	Shaker Body Displacement
x_{cal}	Calibration Mass Displacement
Z	Difference Between x_{DUT} and x_{arm}

Introduction

Vibration qualification tests are performed to ensure that critical components will function properly in their operational vibration environment. They were first performed in the defense industry during World War 2 [1]. Early test standards only prescribed sine testing methods, though methods for random vibrations were added soon after [2]. The first military standard for vibration qualification tests, MIL-STD-810 [3], was released in 1962. Sequential single axis tests with generic straight line specifications were recommended as the standard. Changes have been made to the standard over time, e.g., the recommendation for multi-axis tests in [4], though tests today are largely performed in the same manner as recommended in the first military standard.

1.1 Problems with Standard Tests

Sequential single axis testing with straight-line specifications that may or may not be based on the components actual flight environment remains the standard because it is a simple and repeatable procedure. The method has a few significant weaknesses that have been long known, e.g., being described as early as 1963 in [5]. The three main weaknesses are the enveloping practice, the impedance mismatch, and insufficient actuation, and these problems, along with some potential solutions, are described in further detail below.

1.1.1 Enveloping

Enveloping, or the practice of creating a new specification by exceeding the measured flight environment acceleration power spectral density (PSD) curve with straight lines, used to be a necessity due to limitations in data acquisition and system modeling technologies. It is also somewhat necessary currently as flight data is not always available for components and because components are exposed to a variety of different environments, e.g., the boost portion of a flight, stage separation, and rocket re-entry, so enveloping can be used to increase test level severity so that only a single test can be performed.

Despite its usefulness, it has long been suspected to cause severe over-testing, particularly at fixed base resonances of the device under test (DUT) [6]. One solution to enveloping is to measure the operational environment in flight. Modern data acquisition capabilities make this more reasonable than it used to be, though flight tests are still expensive

[1] Rizzo *et al.*, "The History of a Decision: A Standard Vibration Test Method for Qualification," 2017.

[2] Skousen *et al.*, "Actual Field Response Simulation Using Modified Laboratory Loading Conditions," 2023.

[3] "Military Standard Environmental Test Methods for Aerospace and Ground Equipment," 1962.

[4] "Department of Defense Test Method Standard Environmental Engineering Considerations and Laboratory Tests," 2008.

[5] Salter, "Problem Areas in Dynamic Testing," 1963.

[6] Scharton, "Force Limited Vibration Testing Monograph," 1997.

and might not even include the final version of the hardware being tested. Hence, there have been efforts to estimate flight environments using models of the flight system. These efforts seem to have started at NASA in the 1960s [7–9]. Since finite element modeling [10] was only beginning to be developed then, these early methods did not involve extensive modeling of the flight vehicle or component, but rather focused on modifying previous flight measurements using ratios of component and supporting structure masses, for example.

Recent environment estimation methods utilize improved modeling capabilities to estimate environments at multiple locations on the DUT. These methods generally involve projecting the available measurements onto a set of basis functions, e.g., mode shapes [11], frequency response functions (FRFs) [12], singular vectors of FRFs [13], or even chebyshev polynomials [14], and then using the responses of the basis functions to obtain the physical response at unknown locations. These methods can work well, though they require having some data already available and are prone to error if the set of basis functions being projected onto is ill-conditioned.

1.1.2 Impedance Mismatch

In flight, the DUT is usually attached to a somewhat compliant supporting structure or "next assembly". In single axis tests, the DUT is attached to a rigid fixture which is attached to a (usually very heavy) shaker armature. A single accelerometer is usually placed on the fixture near the base of the DUT, and its acceleration response is controlled by the shaker. Because of the difference in boundary conditions between the flight and lab configuration, excessive force is usually delivered to the DUT in the lab configuration, resulting in an over-test [6].

A potential solution is to design a dynamically active test fixture that matches the mechanical impedance, or force / velocity FRF, of the in flight next assembly. Efforts to do so have been summarized in [15]. The first efforts also seem to have been at NASA in the 1960's [16] and were focused on matching the average impedance and modal spacing of the next assembly. More recent efforts have utilized topology optimization [17–20] to attempt to match various quantities of interest, e.g., FRFs measured on the next assembly, static stiffness of the next assembly, and mode shapes of the next assembly. It is still unclear, though, how effective these fixtures are at improving environment reconstruction; in [18], they were found to increase error due to the increased challenge of controlling more active modes. An improvement in stress reconstruction seemed to be observed in [17]; many of these studies, though, do not give a comparison of test results with a rigid fixture and with the dynamic fixture, so it is hard to tell how effective these designs are. Hence, more research is needed in this area to understand when improved environment reconstruction can be expected.

[7] Barrett, "Techniques for Predicting Localized Vibratory Environments of Rocket Vehicles," 1963.

[8] Klein *et al.*, "The Development of Vibration Test Specifications for Spacecraft Applications," 1965.

[9] Archer, "Structural Vibration Prediction," 1970.

[10] Hughes, *The Finite Element Method: Linear Static and Dynamic Finite Element Analysis*, 2000.

[11] O'Callahan *et al.*, "System Equivalent Reduction Expansion Process," 1989.

[12] Janssens *et al.*, "Experimental example of the pseudo-forces method used in characterisation of a structure-borne sound source," 2002.

[13] Mayes *et al.*, "Predicting System Response at Unmeasured Locations," 2020.

[14] Chen *et al.*, "Non-Model Based Expansion from Limited Points to an Augmented Set of Points Using Chebyshev Polynomials," 2019.

[6] Scharton, "Force Limited Vibration Testing Monograph," 1997.

[15] Taylor *et al.*, "A Comprehensive Review of Efforts to Improve Dynamic Environment Test Fixtures," 2023.

[16] Scharton, "Development of impedance simulation fixtures for spacecraft vibration tests," 1969.

[17] Schoenherr *et al.*, "Improve Replication of In-service Mechanical Environments," 2018.

[18] Rohe *et al.*, "Comparison of Multi-Axis Testing of the BARC Structure with Varying Boundary Conditions," 2019.

[19] Taylor *et al.*, "PDADyE Applied to a 2-attachment Fixture Case," 2024.

[20] Meyer *et al.*, "A Genetic Algorithm-Based Approach for Designing a Fixture that Preserves the Desired Dynamics of a Connecting Part," 2024.

[18] Rohe *et al.*, "Comparison of Multi-Axis Testing of the BARC Structure with Varying Boundary Conditions," 2019.

[17] Schoenherr *et al.*, "Improve Replication of In-service Mechanical Environments," 2018.

1.1.3 Insufficient Actuation

An additional problem with single axis testing is that actual environments usually involve motion in all 6 rigid body degrees of freedom, and it is not possible to control the 6 rigid body degrees of freedom using only a single shaker. This can potentially result in an undertest for sequential single axis testing as the stress simulated in different directions usually adds together, so simulating multiple directions of vibration simultaneously should increase stress. This idea seems to be supported by the results in [21–23], where sequential single axis tests were compared to simultaneous multi-axial excitation. Hence, even if the actual environment is known and a perfect, dynamic test fixture is used, error would still be expected in single axis tests in general as typical environments are not fully controllable with only a single shaker.

1.2 Impedance Matched Multi-Axis Testing

The Impedance Matched Multi-Axis Testing (IMMAT) framework, proposed in [24], mitigates the impedance mismatch and under-actuation problems by including a portion of the operational next assembly in the lab test and by attaching multiple modal shakers to the DUT to excite multi-axial motion. As a result, these tests have shown the potential for improved environment reconstruction, e.g., in [25, 26]. The Transmission Simulator-IMMAT (TS-IMMAT) framework [27] was developed as an alternative to IMMAT when data is available on the next assembly only and not the DUT, and it also demonstrated improved response reconstruction relative to single axis tests.

An obstacle to implementation of IMMATs and TS-IMMATs is that they require increased test planning. One must decide, for example, how many accelerometers should be used and where they should be placed, how many shakers should be used and where they should be placed, as well as how much of the operational supporting structure should be included in the lab test. In addition, smaller modal shakers are used in these tests, and the appropriate size of shaker must be selected so that the test can run without exceeding shaker forcing limits.

Most of these questions have been studied to some extent, e.g., accelerometer selection in [28, 29], shaker location selection in [30, 31], and next assembly selection in [32], though some aspects of IMMAT planning remain ambiguous. For example, there is no general guidance for the number of shakers to use in a lab test, as existing methods rely on optimization algorithms that continue adding shakers until the error is reduced to an acceptable level. In addition, the next assembly study found that including more of the next assembly improved response reconstruction, though it was only performed for a single system, so its conclusion might not hold generally. Finally, existing methods for estimating shaker voltage require either drive point FRFs at connection degrees of freedom on the lab test setup, which can be difficult to obtain and are not usually available, or an accurate modal model of the lab test setup, which may also be unavailable.

[21] Whiteman *et al.*, “Fatigue Failure Results for Multi-Axial Versus Uniaxial Stress Screen Vibration Testing,” 2002.

[22] French *et al.*, “A Comparison of Simultaneous and Sequential Single-Axis Durability Testing,” 2006.

[23] Gregory *et al.*, “Comparison of the Response of a Simple Structure to Single Axis and Multiple Axis Random Vibration Inputs,” 2008.

[24] Daborn, “Smarter dynamic testing of critical structures,” 2014.

[25] Mayes *et al.*, “Physical Vibration Simulation of an Acoustic Environment with Six Shakers on an Industrial Structure,” 2016.

[26] Roberts *et al.*, “Multi-axis vibration testing of an aerodynamically excited structure,” 2018.

[27] Schumann *et al.*, “Transmission Simulator Based MIMO Response Reconstruction,” 2022.

[28] Beale *et al.*, “Degree of Freedom Selection Approaches for MIMO Vibration Test Design,” 2023.

[29] Khan *et al.*, “Evaluating Degree of Freedom Selection Methods for MIMO Vibration Modeling,” 2024.

[30] Rohe *et al.*, “Strategies for Shaker Placement for Impedance-Matched Multi-Axis Testing,” 2020.

[31] Mayes *et al.*, “Optimization of Shaker Locations for Multiple Shaker Environmental Testing,” 2020.

[32] Hall, “Analytically Investigating Impedance-Matching Test Fixtures,” 2020.

1.3 Contributions of Thesis

The contributions of this thesis are aimed at the problems identified in the preceding discussion and are as follows:

1. Understand how much of the next assembly should be included in the lab test.
2. Develop a simplified method for predicting required shaker voltage in multi shaker tests.
3. Understand how many shakers should be used to guarantee accurate response reconstruction in multi-shaker tests.

The next assembly selection question is addressed in Chapter 2. The simplified shaker voltage prediction method is presented in Chapter 3. The number of shakers to use in these tests is addressed in Chapter 4, and overall conclusions are given in Chapter 5.

Next Assembly Selection

This chapter is composed from a paper entitled “Balancing Impedance and Controllability in Response Reconstruction with TS-IMMAT” accepted by the journal *Experimental Techniques* in 2023 [33]. I hereby confirm that the use of this article is compliant with all publishing agreements.

[33] Tuman *et al.*, “Balancing Impedance and Controllability in Response Reconstruction with TS-IMMAT,” 2023.

The theory section of this chapter was primarily written by Matt Tuman and Matt Allen, though it is reproduced here for context. The rest of the chapter was primarily written by the thesis author.

2.1 Theory

Consider the environment reconstruction problem shown in Fig. 2.1, where we wish to reconstruct the operational response on a subcomponent S in the laboratory using a set of shakers. Two possibilities exist: 1.) The response on the subcomponent or on a substantially similar one is measured in the operational environment or 2.) The response is measured near the subcomponent of interest. The former case is depicted in Fig. 2.1 and the latter is depicted in Fig. 2.2. The case depicted in Fig. 2.2 is termed the Transmission Simulator IMMAT method in this work. Both approaches will be discussed in the subsections that follow.

2.1.1 Traditional Environment Reconstruction

When measurements are available on the subcomponent S , then a traditional response reconstruction approach can be used. The essence of the process is described below.

The response of a linear system is related to the applied forces through the frequency response function (FRF) (or matrix of frequency response functions) as follows:

$$\{X_S(\omega)\} = [\mathbf{H}_{S,i}^{S+TS+V}(\omega)]\{F_i(\omega)\}. \quad (2.1)$$

The subscript of \mathbf{H} denotes that it relates the forcing at input locations i to the response at measurement points S , while the superscript indicates that the frequency response is that of the assembly of the subcomponent, S , transmission simulator, TS , and vehicle, V . In this thesis, “transmission simulator” refers to the local supporting structure of the subcomponent or DUT. All FRFs in future equations will be written similarly: i.e., the subscripts will refer to the response and force locations, respectively,

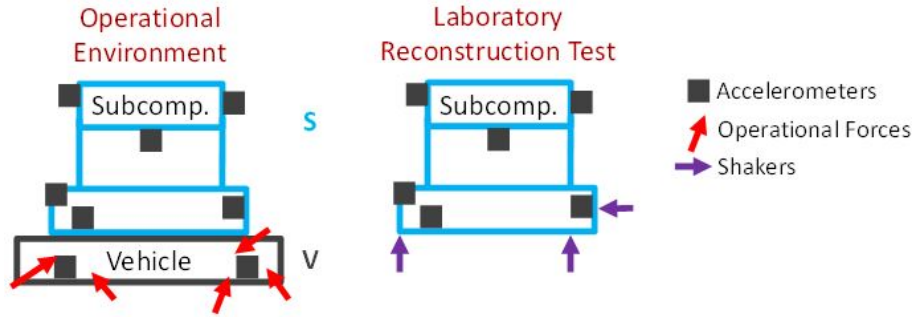


Figure 2.1: Schematic of a traditional environment response reconstruction problem in which measurements are taken on a subcomponent of interest (S) when it is connected to a vehicle (V). In the laboratory, we seek to reconstruct the measured operational environment at a set of measurement points using shakers.

while the superscripts will refer to the component dynamics that are included in the FRF. Implicit in this equation is the number of forces and the locations at which they are applied. If the number and location of the forces is adequate then one can invert the FRF matrix to find the forces that the shakers must apply to reconstruct the desired environment $\{X_s(\omega)\}$,

$$\{F_i(\omega)\} = [\mathbf{H}_{S,i}^{S+TS+V}(\omega)]^+ \{X_s(\omega)\}, \quad (2.2)$$

where $^+$ is the Moore-Penrose pseudoinverse. Note that in the end we wish to replicate the power spectrum of the response $[\mathbf{S}_{X_s X_s}(\omega)] = E(\{X_s(\omega)\} \{X_s(\omega)\}^*)$, where E is the expected value, or average over many measurements, but for the derivation below it is sufficient to consider a single realization of the response.

In practice, the vehicle is not available for the environment reconstruction test, so the system to be inverted is different (i.e., it consists of the subcomponent, S , transmission simulator, TS , and shaker dynamics, Sh , or $[\mathbf{H}_{S,i}^{S+TS+Sh}(\omega)]$) but the desired response can again be obtained so long as the FRF matrix is well conditioned.

$$\{F_i(\omega)\} = [\mathbf{H}_{S,i}^{S+TS+Sh}(\omega)]^+ \{X_s(\omega)\} \quad (2.3)$$

However, there are several well-known difficulties that can be encountered:

- The force required may exceed the limits of the shaker(s).
- The temporal / frequency characteristics of the field forces on the TS may be difficult to replicate with the lab shakers, i.e., it may be challenging to control the TS input motion to the subcomponent through the desired bandwidth.
- Given N_s shakers, one can only guarantee that the response will be matched at N_s points on the structure, but the control can be applied in the least squares sense to produce the closest match that is possible with the given set of shakers.

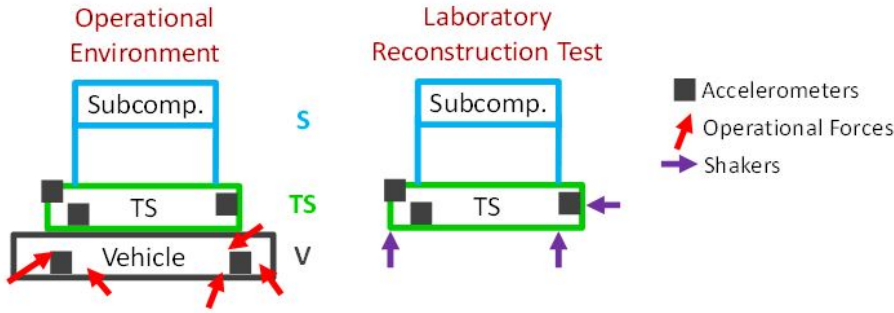


Figure 2.2: Schematic of a TS-IMMAT response reconstruction problem in which a subcomponent of interest (S) is connected to a vehicle (V) through a fixture called a Transmission Simulator (TS). In the laboratory, we seek to reconstruct the measured operational environment using shakers.

One can minimize these issues by choosing the shaker locations and add or redesigning the fixturing to change the FRF matrix $[\mathbf{H}_{S,i}^{S+TS+Sh}(\omega)]$, although the literature contains relatively few guidelines or case studies to help inform these efforts. The present work focuses on an alternative, known as the Transmission Simulator IMMAT method.

2.1.2 Environment Reconstruction with TS-IMMAT

In order to understand the limitations of the TS-IMMAT method, it is helpful to elaborate on the theory that was presented in [27].

In operation, the assembly that consists of a subcomponent of interest, S , connected to a vehicle, V , through a transmission simulator, TS , is excited by forces $\{F_v(\omega)\}$, producing a response on the transmission simulator, $\{X_{TS}(\omega)\}$, which we wish to replicate. The forces are related to the response via a frequency response function $[\mathbf{H}_{TS,V}^{S+TS+V}(\omega)]$. The subscript denotes that this FRF relates forces on the vehicle, V , to response on the transmission simulator, TS , and the superscript $S+TS+V$ suggests that the shaker, transmission simulator, and vehicle dynamics are again included in this FRF.

[27] Schumann *et al.*, "Transmission Simulator Based MIMO Response Reconstruction," 2022.

$$\{X_{TS}(\omega)\} = [\mathbf{H}_{TS,V}^{S+TS+V}(\omega)]\{F_V(\omega)\} \quad (2.4)$$

We assume that measurements were only acquired on the transmission simulator, although we will also speak of the response, $\{X_S(\omega)\}$, of the system of interest since these are the responses that we actually want to replicate. A MIMO test is used in which forces, $\{F_{TS}(\omega)\}$, are applied to the transmission simulator, with the goal of replicating the measured response.

$$\begin{Bmatrix} X_S^{lab} \\ X_{TS}^{lab} \end{Bmatrix} = \begin{bmatrix} \mathbf{H}_{S,TS}^{S+TS+Sh}(\omega) \\ \mathbf{H}_{TS,TS}^{S+TS+Sh}(\omega) \end{bmatrix} \{F_{TS}(\omega)\}, \quad (2.5)$$

$$\begin{Bmatrix} X_S^{true} \\ X_{TS}^{true} \end{Bmatrix} = \begin{bmatrix} \mathbf{H}_{S,V}^{S+TS+V}(\omega) \\ \mathbf{H}_{TS,V}^{S+TS+V}(\omega) \end{bmatrix} \{F_V(\omega)\}. \quad (2.6)$$

Using the bottom two rows to equate $\{X_{TS}^{lab}(\omega)\} = \{X_{TS}^{true}(\omega)\}$, we find the forces that the MIMO controller must apply to match the response on the transmission simulator.

$$\{F_{TS}(\omega)\} = ([\mathbf{H}_{TS,TS}^{S+TS+Sh}(\omega)])^{-1}[\mathbf{H}_{TS,V}^{S+TS+V}(\omega)]\{F_V(\omega)\} \quad (2.7)$$

In practice we aren't concerned with this equation because the controller takes care of computing the forces to match the responses on the transmission simulator, but we can use this equation to determine whether it is possible for the controller to achieve an adequate match with the number of shakers and shaker locations that are available. The power spectrum of the TS response, computed using the last two terms in the preceding equation, provides some insight.

$$[\mathbf{S}_{X_{TS}X_{TS}}(\omega)] = [\mathbf{H}_{TS,V}^{S+TS+V}(\omega)][\mathbf{S}_{F_V F_V}(\omega)][\mathbf{H}_{TS,V}^{S+TS+V}(\omega)]^* \quad (2.8)$$

There could be many forces exerted on the vehicle, so the dimensions of the matrix $\mathbf{S}_{F_v F_v}(\omega)$ could be much larger than those of $\mathbf{S}_{X_{TS}X_{TS}}(\omega)$, exciting many dynamics that cannot be fully observed on the TS. Furthermore, many modes may be active in $[\mathbf{H}_{TS,V}^{S+TS+V}(\omega)]$, adding more complexity to the response $[\mathbf{S}_{X_{TS}X_{TS}}(\omega)]$. For the transmission simulator method to work, the response $[\mathbf{S}_{X_{TS}X_{TS}}(\omega)]$ must be spanned by its first N_{TS} mode shapes. If that is the case, and if there are at least N_{TS} sensors so that one can capture those modes, then the power spectrum $[\mathbf{S}_{X_{TS}X_{TS}}(\omega)]$ can be reproduced. This requires that we apply at least N_{TS} forces to the system. In the studies in this work $N_{TS} = 6$ because the transmission simulator is rigid, which means that we can only reproduce the response of six modes at each frequency line. In [34], the authors asserted that the free-free mode shapes of the TS could form an adequate basis for reconstructing the response of the TS, $\{X_{TS}(\omega)\}$.

[34] Tuman *et al.*, "Investigation of Transmission Simulator-Based Response Reconstruction Accuracy," 2022.

$$\{X_{TS}(\omega)\} = \sum_{r=1}^{N_{TS}} \frac{\phi_{TS}^{TS}(\phi_{TS}^{TS})^T \{F_{TS}(\omega)\}}{(\omega_r^{TS})^2 - \omega^2 + i\omega 2\zeta_r^{TS} \omega_r^{TS}} + \sum_{r=N_{TS}+1}^{\infty} \frac{\phi_{TS}^{TS}(\phi_{TS}^{TS})^T \{F_{TS}(\omega)\}}{(\omega_r^{TS})^2 - \omega^2 + i\omega 2\zeta_r^{TS} \omega_r^{TS}} \quad (2.9)$$

In the above, the first term represents the sum of the N_{TS} modes that we are able to control and the second term is the error due to all of the modes that cannot be controlled because there are not enough shakers. There also could be error in the first term due to imperfection in the controller, especially when the controller limits the applied force by truncating singular values. In either case, one can expect that there will be error in the reconstruction on the TS.

$$\{X_{TS}(\omega)\} = \{X_{TS}^{true}(\omega)\} + \{e_{TS}\} \quad (2.10)$$

Even if the response on the TS was reconstructed perfectly, we still might not reproduce the response perfectly on the subcomponent of interest

because the dynamics of the subcomponent can be different in the lab as compared to the field. For example, there may be part-to-part variations between the subcomponent in the field and that present in the true environment. Returning to Eqs. 2.5-2.6, we see that

$$\{X_S^{lab}(\omega)\} = [\mathbf{H}_{S,TS}^{S+TS+Sh}(\omega)]\{F_{TS}(\omega)\} = [\mathbf{H}_{S,TS}^{S+TS+Sh}(\omega)]([\mathbf{H}_{TS,TS}^{S+TS+Sh}(\omega)]^{-1}\{X_{TS}^{lab}(\omega)\}), \quad (2.11)$$

and substituting in the approximation for $\{X_{TS}^{lab}\}$, we obtain the following,

$$\{X_S^{lab}(\omega)\} = [\mathbf{H}_{S,TS}^{S+TS+Sh}(\omega)]([\mathbf{H}_{TS,TS}^{S+TS+Sh}(\omega)]^{-1}(\{X_{TS}^{true}(\omega)\} + \{e_{TS}\}), \quad (2.12)$$

which we hope will be a good approximation of the true response,

$$\{X_S^{true}(\omega)\} = [\mathbf{H}_{S,V}^{S+TS+V}(\omega)]([\mathbf{H}_{TS,V}^{S+TS+V}(\omega)]^{-1}\{X_{TS}^{true}(\omega)\}). \quad (2.13)$$

This shows that the error in $\{X_S^{true}\}$ can arise from two sources: 1.) Error in reconstructing the response on the TS, due to the term $\{e_{TS}\}$ and 2.) Differences in the transmissibility $[\mathbf{H}_{S,V}^{S+TS+V}(\omega)]([\mathbf{H}_{TS,V}^{S+TS+V}(\omega)]^{-1}$ between the assembly on the vehicle and that in the laboratory $[\mathbf{H}_{S,TS}^{S+TS+Sh}(\omega)]([\mathbf{H}_{TS,TS}^{S+TS+Sh}(\omega)]^{-1}$. Note that the first source of error depends strongly on the number of shakers that are available; if there are not enough shakers available to fully control the TS then it may be impossible to make the term $\{e_{TS}\}$ sufficiently small.

In our prior work [34], and again in the results that will be presented here, we have found that these two sources of error are important. Specifically, the results show that even when the response of the TS was reconstructed quite well, the response of the system of interest still has significant errors.

[34] Tuman *et al.*, "Investigation of Transmission Simulator-Based Response Reconstruction Accuracy," 2022.

2.1.3 Reconstruction Error Metrics

In the results that follow, two error metrics were used to quantify the difference between the target environment and that achieved in the laboratory. The average dB difference of two ASDs for all relevant accelerometer channels at a frequency line is defined as follows.

$$e_{ASD}(f_i) = \sqrt{\frac{1}{n_{accels}} \sum_{k=1} n_{accels} [dB[\mathbf{S}_{X_k X_k}(f_i)] - dB[\mathbf{S}_{X_k X_k, lab}(f_i)]]^2} \quad (2.14)$$

For this work, $[\mathbf{S}_{X_k X_k, lab}(f_i)]$ is the simulated or experimental acceleration ASD for the k th accelerometer DOF and $[\mathbf{S}_{X_k X_k}(f_i)]$ is the operational ASD for the same DOF. After computing an error value for each frequency line, a final metric is computed using,

$$e_{ASD} = \sqrt{\frac{1}{n_{freq}} \sum_{i=1}^{n_{freq}} e_{ASD}(f_i)^2}. \quad (2.15)$$

This final error number represents the RMS dB error across all accelerometers and frequency lines. A low error metric communicates a successful reconstruction test; this metric will be used moving forward to compare various tests.

This error metric was used to create a shaker placement algorithm, detailed in Appendix A, that was used to select optimal shaker locations for various tests that were performed in the precursor to this work [34]. While that method was found to be effective, over various tests it was found that the results were not very sensitive to the shaker locations so long as an acceptable set was found; in other words, there were many possible sets of shaker locations that gave similar results. Hence, to simplify the presentation in this work, a single set of shaker locations was used that was selected based on experience and engineering judgement.

[34] Tuman *et al.*, "Investigation of Transmission Simulator-Based Response Reconstruction Accuracy," 2022.

2.2 Experimental Case Study

To further evaluate the TS-IMMAT methodology, it was tested on the system shown in Fig. 2.3. The photo shows the most complicated subsystem considered. The actual flight configuration consisted of the assembly shown with data acquisition systems bolted onto the bulkhead plate, and the whole assembly was bolted to a fiberglass tube and into the sounding rocket. In a previous work, reconstruction tests were performed using assemblies with the same plate (TS) and stool (subcomponent); however, these assemblies did not include the pillars or the bottom bulkhead. The accelerometers are positioned in a cylindrical coordinate system, and the directions referenced throughout the rest of this analysis are specified in Fig. 2.3. This assembly flew inside a sounding rocket flown for Kansas City National Security Campus in July 2019. The assembly was instrumented with three triaxial accelerometers on the plate and three triaxial accelerometers on the stool. During flight, the rocket experienced four main phases: boost, coast, deployment of the drogue parachute, and deployment of the main parachute. The operational environment power spectral density (PSD) profiles were constructed from acceleration time data from 0.5 to 20 seconds after launch. This time frame captures the boost and coast phase while excluding any shock event at ignition along with the deployment of the parachutes.

The frequency spacing of the PSD profiles generated was 5 Hz, and the testing bandwidth of interest was 100 to 4000 Hz. Unfortunately, the data from the first accelerometer in the radial direction (channel 1) only recorded noise during flight. Thus, there are eight channels on the plate and nine channels on the stool that recorded useful data.

Three assemblies will be considered in the following analysis, and the test setups for each assembly are shown in Fig. 2.4. For each configuration, the goal is to reconstruct the environment on the plate using six small shakers using MIMO control. To assess the success of a TS-IMMAT test for each configuration, the accuracy of response on the controlled plate and on the uncontrolled stool will be compared. Our prior work [27] presented TS-IMMAT reconstruction tests on Configurations A and B; this

[27] Schumann *et al.*, "Transmission Simulator Based MIMO Response Reconstruction," 2022.

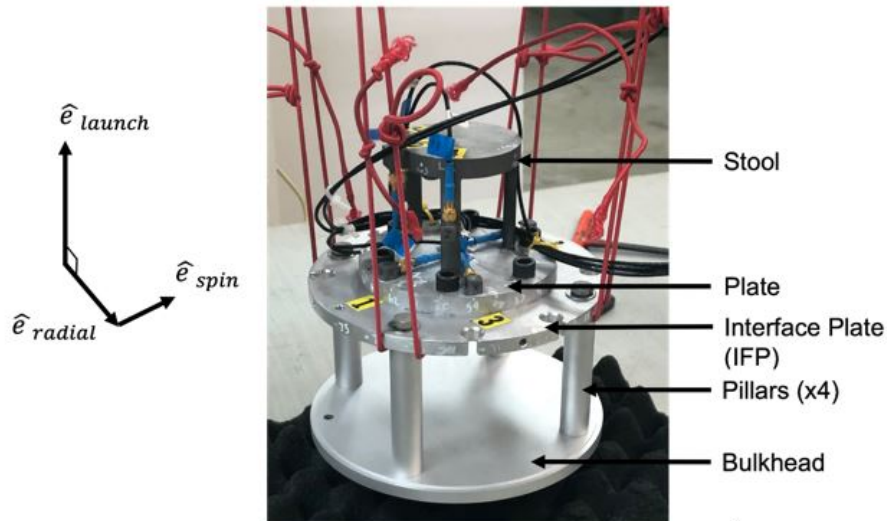


Figure 2.3: The instrumented next-level assembly

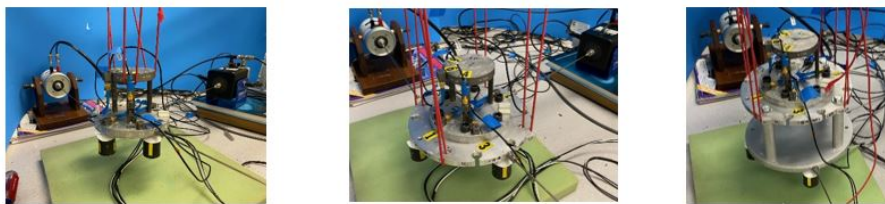


Figure 2.4: The three assemblies tested are Configuration A with the stool and plate, Configuration B with the stool, plate, and IFP, and Configuration C with the stool, plate, IFP, pillars, and bulkhead

work will focus on comparing those with Configuration C. Furthermore, the results will be evaluated in light of the theory presented previously.

2.2.1 Roving Hammer FRFs

To be able to simulate a MIMO test, the frequency response functions, e.g., in the top line of Eq. 2.5, are needed. These were obtained by performing a roving hammer test on each configuration. For each configuration, the structure was excited at various locations and the response was measured. Data Physics Abacus hardware and SignalCalc 730 software recorded the FRFs in the bandwidth of 0 to 4000 Hz with a frequency resolution of 5 Hz to match the environmental acceleration profiles. While these FRF's could be used to select an optimal set of shaker locations, we used the locations shown in Fig. 2.4 to maintain consistency between setups. Thus, the MIMO tests were simulated using the portions of the FRF corresponding to the chosen shaker locations, and these results are shown later to demonstrate the accuracy of the simulations. It's worth noting that this FRF does not account for the dynamics of the shakers that are attached to the device under test. Thus, the roving hammer FRF

is an approximation of the MIMO test FRF, and some error is expected in the simulation predictions.

2.2.2 Experimental Methodology

The workflow for performing a TS-IMMAT reconstruction test is as follows. The measured FRFs are used to simulate the MIMO test using the top line of Eq. 2.5. To compare test results between different configurations more accurately, similar sets of shaker locations were used on each configuration. The simulated test results are discussed later, to give an idea of how accurate these simulations are.

Then, to perform the actual MIMO test, shakers were attached at the desired locations. Three SIEMENS Q-MSH electromagnetic (EM) inertial shakers were used to excite the assembly in the launch direction. These three shakers were attached directly to the structure using super glue. In the non-launch directions, two Modal Shop EM shakers and one Ling Dynamics (LDS) EM shaker were connected to the assembly via stingers made of piano wire which were also attached with super glue. For each configuration, the Modal Shop shakers excited the structure radially, and the LDS shakers were attached to an angle block to excite torsion in the structure. In Configuration A, the shakers were attached to the plate. In Configuration B, the shakers were attached to the interface plate, and in Configuration C, all shakers were attached to the bottom bulkhead.

To perform the MIMO test, Data Physics Abacus hardware and Data Physics SignalStar Matrix controller software were used. Per requirements of the TS-IMMAT approach, the closed-loop MIMO software only controlled to the accelerometers on the plate. Because one accelerometer channel recorded noisy data during flight and another channel started to record poor measurements in the laboratory, only seven accelerometer channels were controlled to. The control profiles were the PSD matrices constructed from the flight data as described earlier. The remaining 9 accelerometer channels on the stool were not controlled to, but they were measured.

2.2.3 MIMO Test Results

Figure 2.5 presents the auto-spectral densities (ASD's) for the accelerometer channels on the controlled plate. The black line is the operational environment profile that is being controlled to, and the cyan line is the response recorded during the reconstruction test. Additionally, for each channel, the dB error computed using Eq. 2.15 is provided in each subplot's title.

The reconstruction on the plate was relatively accurate throughout the testing bandwidth, having an RMS error of 7.2 dB. While we presume that one would not have measurements on the component of interest in practice, we had accelerometers on the stool so we could evaluate the performance of the proposed TS-IMMAT approach. Figure 2.6 illustrates the measured ASD's of the accelerometer channels on the stool (cyan) with the environment profiles generated from the flight data (black).

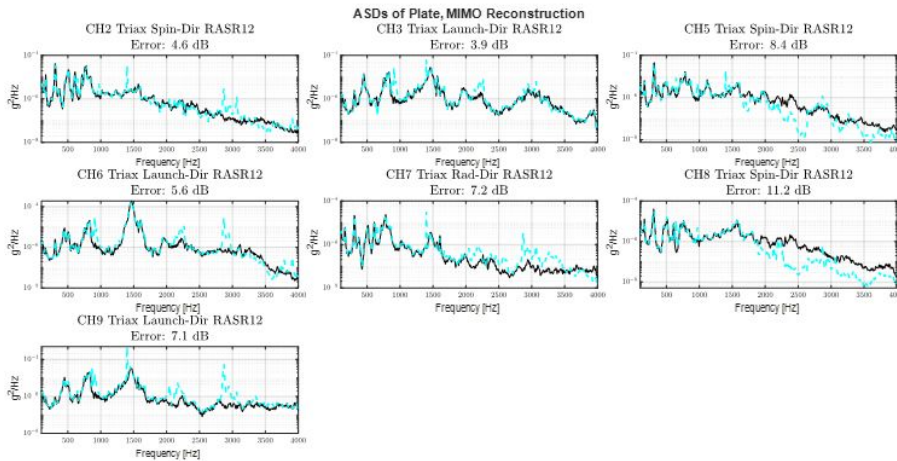


Figure 2.5: Reconstruction ASDs of the controlled accelerometers on the plate (cyan) along with the control ASDs (black) for Configuration C

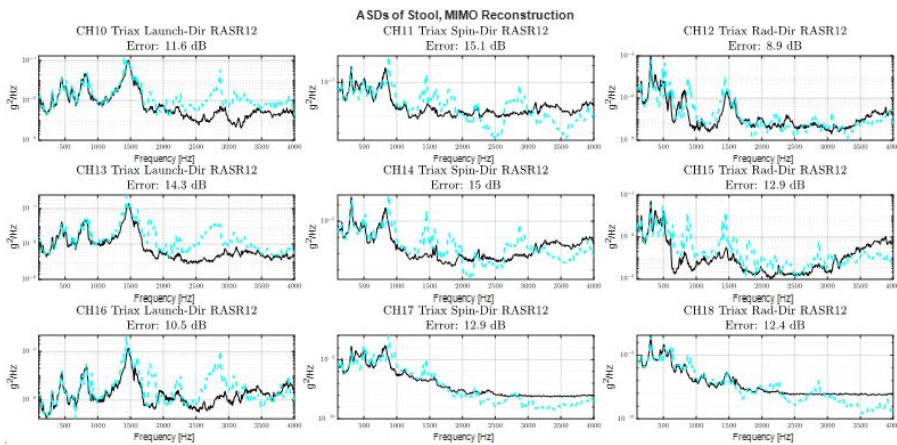
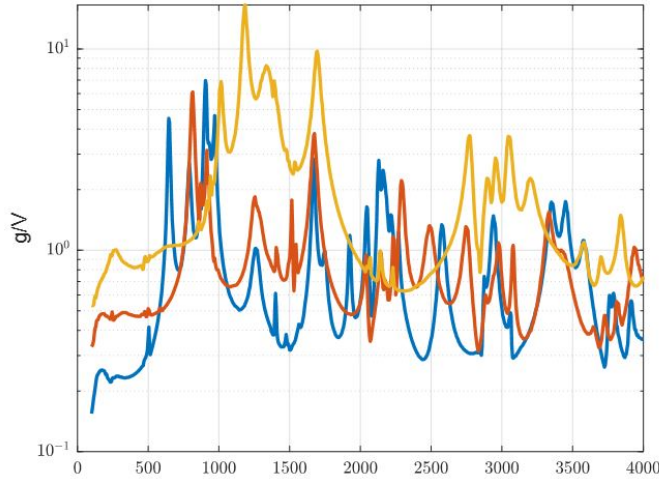


Figure 2.6: Measured ASDs of the uncontrolled accelerometers on the stool (cyan) along with the environment ASDs (black) for Configuration C

Unsurprisingly, the error in reconstructing the stool response is higher than the error in reconstructing the plate response. Up to 500 Hz, the error is relatively low, but it increases significantly at higher frequencies, presumably due to a larger number of active elastic modes. Thus, the total error in the bandwidth is a higher 12.8 dB. It is interesting to compare these results to those obtained on Configurations A and B. Table 2.1 compares the error metric obtained in each of these configurations from 100 to 2000 Hz and 100 to 4000 Hz. Each of these tests was performed with a condition number threshold of .01 to reduce the voltage levels required for each shaker. An in depth discussion of the condition number threshold is given later in this paper. It is worth noting that all configurations give very similar results in the 100-2000 Hz frequency band, and there are only a few differences for the 100-4000 Hz range.

Table 2.1: Error in experimental reconstruction for three assemblies tested

Assembly	Error from 100-2000 Hz (dB)		Error from 100-4000Hz (dB)	
	Plate	Stool	Plate	Stool
Configuration A	2.5	10.1	3.1	11.2
Configuration B	2.0	11.2	2.9	14.3
Configuration C	3.4	11.3	7.2	12.8

**Figure 2.7:** Composite of the Frequency Response Functions measured on each of the configurations: (yellow) Configuration A, (red) Configuration B, (blue) Configuration C

Discussion

First consider the controllability of each assembly. The control was applied only to the plate accelerometers, and the controller was able to match their responses very accurately in all cases except for Configuration C at higher frequencies. The composite frequency response of each configuration is shown in Figure 2.7, which shows that Configurations A and B have far fewer active modes than Configuration C, explaining this difference. However, the far more flexible transmission simulator in Configuration C only significantly affects the results above 2000 Hz.

The previous testing of Configuration A and Configuration B suggested that using more of the original operational structure would improve the response accuracy for the controlled transmission simulator (plate) and for the uncontrolled subcomponent (stool). Those results had been obtained using different sets of shaker locations on the two configurations and potentially different settings in the control that limited the effectiveness of the shakers. When these issues were corrected, it is possible to obtain very good control on the plate for all configurations as seen here. In the results above, the accuracy on the stool was similar for all configurations. This suggests that none of these configurations improves the transmissibility of the plate's response to the stool enough to overcome the errors in reconstructing the plate (or TS) response. Hence the error term in Eq. 2.12 seems to be much more significant

Table 2.2: Average Shaker RMS Voltage in Tests Performed on Each Configuration

Assembly	Average Shaker RMS Voltage (V)	
	100-2000 Hz	100-4000 Hz
<i>Configuration A</i>	0.072	0.083
<i>Configuration B</i>	0.105	0.156
<i>Configuration C</i>	0.236	0.281

than error due to noise or limitations of the controller. The errors at the control accelerometers are quite low, as shown in Fig. 2.5. This might suggest that $\{e_{TS}\}$ is also low, but that is only true if enough control accelerometers are available to ensure that all active modes in the TS are accurately captured. This does not seem to be the case. In Fig. 2.6 the response on the stool only tracks the desired environment to 500 Hz or so, so beyond that point we expect that the modes of the TS are active enough to introduce significant errors in the stool.

Only six shakers are available, so at most six modes can be controlled at each frequency line. As shown in Fig. 2.7, the assembly has many more modes as more of the next assembly is added. However, the modes considered in Fig. 2.7 are those of the entire assembly. If one considers only the transmission simulator, then a simple finite element model that was constructed as part of this work places the first flexible mode for Configurations A and B at around 3300 Hz and 2700 Hz respectively. For Configuration C, the pillars and bottom bulkhead are quite flexible which drops the first flexible mode of the TS down to 900 Hz. Therefore, Configuration C is not controllable for a much larger portion of the total bandwidth compared to the other two configurations. This, perhaps, explains the large error term in Eq. 2.9 for Configuration C relative to the lower errors observed for Configurations A and B.

Another important factor to consider in deciding how much of a part's attached structure should be included in a test is the capabilities of the shakers. Since IMMATs use smaller shakers that have lower voltage limits, it is common for these limits to be exceeded, preventing a test from running. As mentioned previously, a condition number threshold of 0.01 was used for the previous tests because some of the shakers' voltage limits would have been exceeded in testing configuration C without the threshold. As seen in Table 2.2, the required shaker voltage increases when more of the attached structure is included in a test. This is not surprising given that including more of the assembly makes the structure heavier, requiring greater shaker force.

Effect of Shaker Locations

It is worth discussing the effect of shaker locations on the reconstruction error. The shakers were placed at the locations used in these tests to avoid some common problems in IMMATs. One is when two shakers are placed opposing each other, resulting in higher required shaker voltage and poorer reconstruction. The locations previously used largely

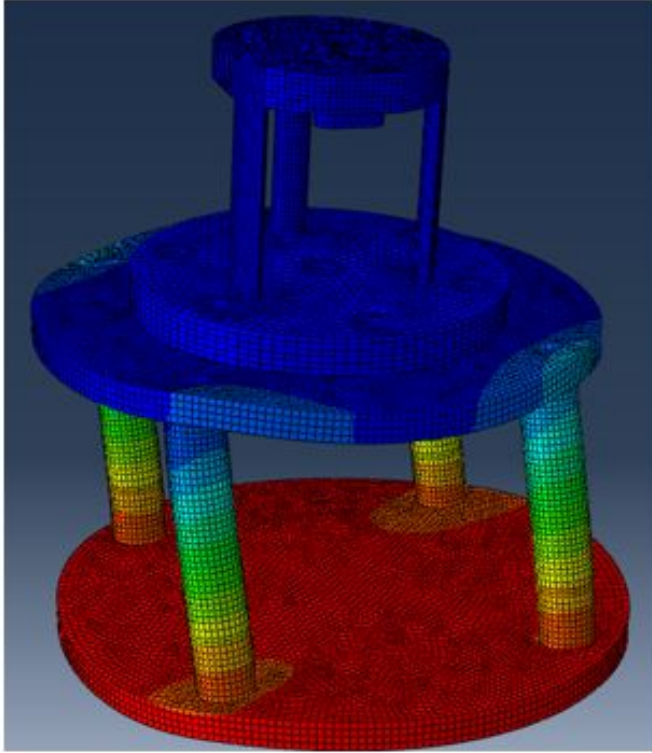


Figure 2.8: 2nd Fixed Plate Mode of Configuration C, 451 Hz

avoided this problem as no shakers directly opposed any others. Another problem is failing to excite the device under test in any of the rigid body degrees of freedom, and the set of shaker locations we used avoids this problem as well, exciting in the radial, spin, and launch directions.

One area of uncertainty, though, was where to place the shakers on configuration C. As shown in Fig. 2.4, we attached the shakers to the bottom bulkhead plate in the previous tests, assuming that this would most accurately match the in-flight load path and yield the most accurate reconstruction. It is possible that there are modes excited in the test, such as the second fixed-plate mode shown in Fig. 2.8, wherein the bottom bulkhead plate and columns deform significantly while the stool does not, though. This mode was obtained by fixing the nodes at the locations of the accelerometers on the plate in a simple FEM of configuration C, and it should represent how the structure deforms when plate accelerometers are controlled to in a test. It seems possible, therefore, that the stool response would be more accurately reconstructed by attaching the shakers to the interface plate instead, as by doing so, the shakers would not have to control these fixed plate modes.

To test this theory, a physical test was performed with the shakers attached to the interface plate on configuration C as shown in Figure 2.9. The shakers were placed roughly at the same locations as the previous test on configuration B. Shorter stingers were used in this test, but we have found that our shakers can control the axial stinger modes well, so

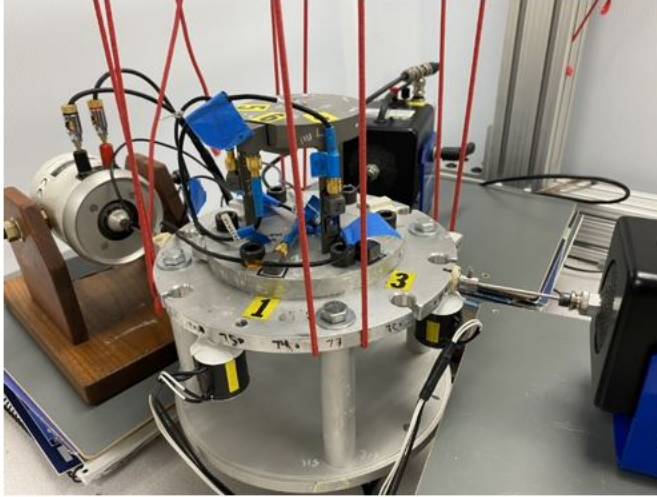


Figure 2.9: Test Setup on Configuration C with Shakers Attached to Interface Plate

Table 2.3: RMS dB Error on Configuration C when Shakers are attached to Bulkhead Plate and Interface Plate

Shaker Locations	Error from 100-2000 Hz (dB)		Error from 100-4000Hz (dB)	
	<i>Plate</i>	<i>Stool</i>	<i>Plate</i>	<i>Stool</i>
<i>Bulkhead Plate</i>	3.4	11.3	7.2	12.8
<i>Interface Plate</i>	4.8	13.0	7.9	14.2

stinger length should not affect the reconstruction error in this case. All other test settings were kept the same, and a condition number threshold of .01 was implemented on the FRF matrix.

As seen in Table 2.3, error does not significantly change when the shakers are attached to the interface plate instead of the bulkhead plate. This again shows how impedance and controllability of the transmission simulator work against each other; attaching shakers to the bulkhead plate matches flight impedance more accurately and excites more modes, while attaching them to the interface plate reduces the number of modes that need to be controlled at the expense of matching the flight load path. Since reconstruction accuracy remains about the same for both sets of shaker locations, we assume that attaching the shakers to the bulkhead is fairly optimal for configuration C and that we are comparing the best results we can obtain on each assembly. It doesn't seem that reconstruction accuracy is very sensitive to changes in shaker locations, provided that the shakers are placed to minimize interactions between them and to excite the structure in all rigid body degrees of freedom.

2.2.4 Configuration B2 – Test with Small Error Term in Eq. 2.9.

The TS-IMMAT theory was further tested by repeating the test on Configuration B while using only three shakers to seek to control all of the modes in the launch direction, as shown in Fig. 2.10. In this direction the first mode of the transmission simulator occurs above 2500 Hz, and

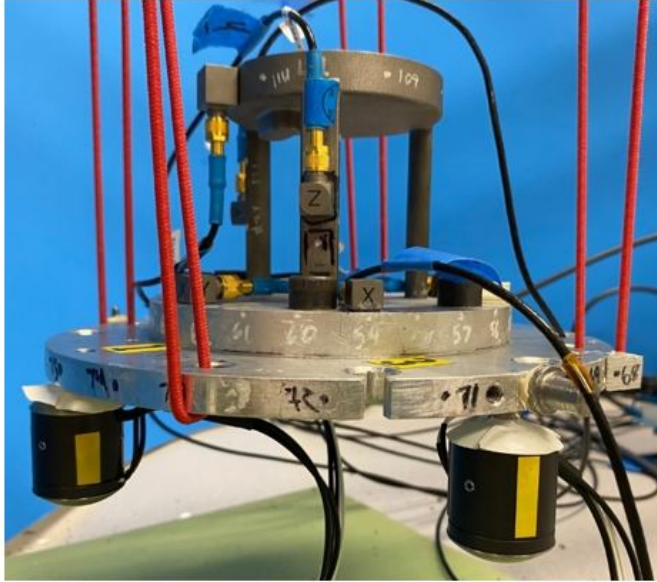


Figure 2.10: Photo of test setup for Configuration B-2 with three shakers in the launch direction and all others removed.

the first mode of the assembly in the launch direction is also above 2500 Hz. Hence, according to the theory presented earlier, one would expect to be able to achieve excellent control of the transmission simulator in the launch direction, and that the system of interest (the stool) should also achieve the desired response.

The results, presented in Fig. 2.11, confirm this hypothesis. Up to 500 Hz, the errors in the launch direction are 0.8 and 2.7 dB RMS on the plate and stool respectively. Thus, the three Q-source shakers reproduce the environment on the plate and stool very accurately at low frequencies. At higher frequencies, the plate response is reconstructed well, but there is significant error near 600 Hz in the stool response, which is in the vicinity of the first bending mode of the assembly. The results slowly degrade above this frequency, and by 2000 Hz, the error grows noticeably as we approach the first axial mode of the plate. The three available shakers are insufficient to control the four modes (three rigid body and one elastic) that are active at this frequency. While there is error at higher frequencies, the reconstruction is quite accurate at low frequencies where rigid body motion dominates, demonstrating that the transmission simulator theory holds true.

2.2.5 Configuration A2 – Test with Small Transmissibility Mismatch in Eqs. 2.12 and 2.13

As mentioned earlier, the second source of error in a TS-IMMAT test is the mismatch in transmissibility (or impedance mismatch) between the lab and true environment. To test the importance of this transmissibility term in Eqs. 2.12 and 2.13, a simple experimental study is performed. Configuration A from Fig. 2.4 was suspended in the laboratory using a

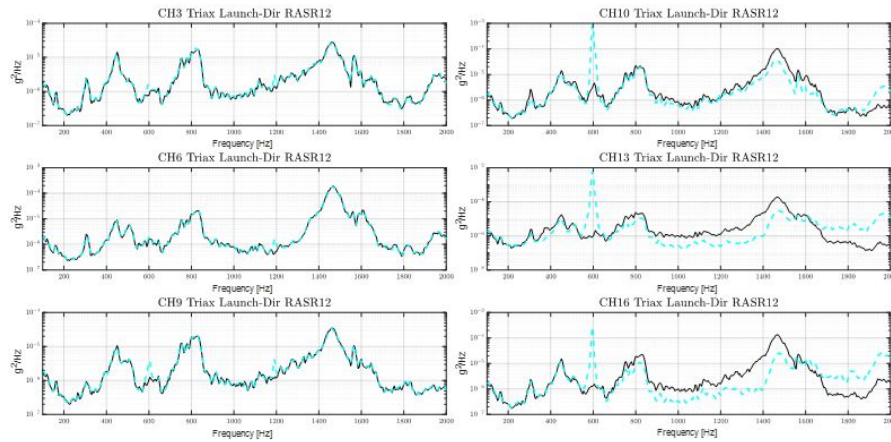


Figure 2.11: Response of the stool on plate system in the launch direction, with Plate accelerometers (CH3, CH6 and CH9) and Stool accelerometers (CH10, CH13 and CH16)

bungee cord suspension system. The plate was then struck randomly for 10 seconds, and time histories from the accelerometers were recorded during these 10 seconds of excitation. These time histories were then used to construct ASDs and CSDs that served as the new operational environment profile. Controlling to this new environment profile, a MIMO test of the same system under the same free-free boundary conditions was performed. Because the system (subcomponent plus TS) exactly matches that which will be used during MIMO control, except for any change in the impedance due to attaching the shakers, the transmissibility should be nearly identical in Eqs. 2.12 and 2.13. In contrast, the error term due to controlling up to 12 modes with 6 shakers could remain as large as it was in the other case studies. A set of shaker locations was chosen to minimize plate response error for the new test profile, and a MIMO test controlling to 7 accelerometers on the plate was then performed, i.e. the TS-IMMAT method because the stool accelerometers were not included in the control. Rather than showing all of the individual spectra, Figure 2.12 presents the average of the measured ASDs (i.e. the trace of the CSD matrix) of the controlled accelerometers on the transmission simulator (left) and the sum of the measured ASDs of the uncontrolled accelerometers on the subcomponent (right).

The results from Configuration A2 show excellent agreement between the desired environment and the reconstruction. Using the dB error metric, the error from 100 to 5000 Hz on the plate and the stool is 5.9 dB and 8.3 dB respectively. The errors are dominated by several single-frequency-line deviations at high frequencies, but these are attributed to noise in the data acquisition and control systems, because this environment was at a much lower amplitude and hence near the noise floor of the systems. Nevertheless, if this is ignored then the results are outstanding in this case study on both the transmission simulator and the object of interest. This suggests that the transmissibility, which is influenced by the boundary

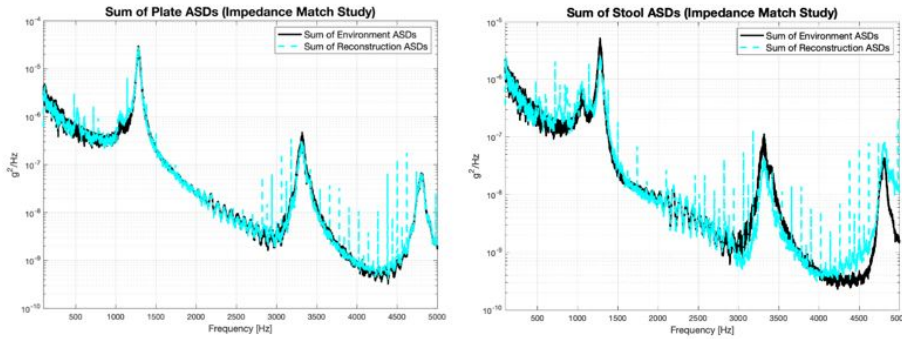


Figure 2.12: Measured ASDs of the plate (left) and the stool (right) from Configuration A-2, the case study where there is a near perfect impedance match between lab and the true environment.

conditions in test, is extremely important. Unfortunately, in most cases of interest one does not have the entire vehicle to test and so the impedance is not likely to match as well as it does in this case study.

2.3 Conclusions

This paper investigated the influence of impedance on the ability to reconstruct a random vibration environment for a component by controlling to accelerometers only on a transmission simulator that the component is attached to. A derivation showed that error in reconstructing an environment using the Transmission Simulator IMMAT method comes from two sources: 1.) a limit in the number of modal degrees of freedom of the TS that can be controlled due to a limited number of shakers, 2.) differences in the transmissibility of the tested assembly between the laboratory and the actual environment of interest. The latter affects how errors at the control accelerometers propagate to other places of interest on the structure. Several case studies were presented to explore the relative importance of these sources.

The results suggest a few interesting conclusions. First, Configuration A-2 showed that, if the impedance can be matched very closely between test and the true environment, that one can obtain very accurate results with relatively little difficulty. However, when even the best configuration available is quite far from the true flight boundary condition (e.g. Configuration C), then it seems to be much more important to limit the number of modes active in the transmission simulator for a fixed set of shakers rather than to try to match the flight boundary condition a little more closely. Specifically, while Configuration C included more of the vehicle, and presumably a closer match in impedance or transmissibility, worse results were obtained when using that Configuration as compared to Configurations A and B, presumably because those configurations had far fewer active modes. The mass-spring case studies clearly illustrated cases where the transmission simulator could be controlled at low frequencies, because the number of modes active was less than or equal

to the number of shakers. At higher frequencies the shakers could not reproduce the environment precisely, and so they matched it at a few points on the structure and this might lead to significant errors at other points depending on the transmissibility of the system.

Shaker Voltage Prediction

This chapter is composed from a paper entitled “A Simplified Method for Predicting Shaker Voltage in IMMATs” submitted to the journal *Experimental Techniques* in 2023 [35]. I hereby confirm that the use of this article is compliant with all publishing agreements.

The thesis author is the primary author of all content in this chapter.

[35] Behling *et al.*, “A Simplified Method for Predicting Shaker Voltage in IMMATs,” 2023.

3.1 Introduction

Because traditional single axis tests often result in over testing, more accurate operational stress replication has been the subject of significant research. Force and response limits have been implemented in single axis tests to reduce over testing at DUT resonances [6]. Six degree of freedom shaker tables have more recently been developed and have shown the ability to accurately reproduce a component’s environment in multiple directions simultaneously [36]. Since component level data is often unavailable for testing, methods have also been developed to reproduce a component’s environment in multiple axes simultaneously using data on the next assembly only [27].

[6] Scharton, “Force Limited Vibration Testing Monograph,” 1997.

[36] Paripovic *et al.*, *Reproducing a Component Field Environment on a Six Degree-of-Freedom Shaker*, 2021.

[27] Schumann *et al.*, “Transmission Simulator Based MIMO Response Reconstruction,” 2022.

As previously mentioned, Impedance Matched Multi-Axis Tests (IMMAT) are another promising alternative. Proposed by Daborn *et al.* [24], they generally involve testing a component attached to some amount of its operational “next assembly”. By attaching modal shakers to various locations on the next assembly, the component’s operational boundary conditions are more closely matched than in a shaker table test, making environment reconstruction more feasible. Typical environments can be reconstructed with much smaller shakers than required for traditional tests as shaker locations can be chosen to minimize the required force [30]. Regularization methods can also help reduce shaker force at the expense of reconstruction accuracy [37, 38]. Even so, it is helpful to be able to predict the force that the shakers must exert so one can select adequate shakers for the application of interest. If the shakers and their locations are not correctly chosen then the shaker’s performance limits can be exceeded, preventing accurate environment reconstruction.

[24] Daborn, “Smarter dynamic testing of critical structures,” 2014.

[30] Rohe *et al.*, “Strategies for Shaker Placement for Impedance-Matched Multi-Axis Testing,” 2020.

[37] Schultz, “A Demonstration of Force Estimation and Regularization Methods for Multi-Shaker Testing,” 2020.

[38] Schultz *et al.*, “Shape-constrained Input Estimation for Efficient Multi-shaker Vibration Testing,” 2020.

Though shaker performance can be limited by multiple factors, including current, force, and other constraints [39], this study will focus on the voltage that is output from the amplifier into the shaker. Accurately predicting shaker voltage requires an accurate model of

[39] Lang *et al.*, “Understanding the Physics of Electrodynamic Shaker Performance,” 2001.

the shaker and DUT. Once these are known, shaker models can be coupled to the DUT via dynamic substructuring. An FRF relating shaker voltage to DUT acceleration at sensor locations is required to simulate the IMMAT and can be obtained from the model of the substructured system. Previous studies have successfully used dynamic substructuring to obtain a coupled model of the shaker-DUT system and predict test success [31, 40, 41].

Though accurate, substructuring and FEM creation are not trivial processes. One may not have sufficient information about the DUT to create a FEM, and so the model for the DUT would need to be created experimentally. Furthermore, most testing labs do not have models for their shakers. Shaker models are more easily calibrated when the electrical current in the shaker can be measured, but current sensors were not available for this study, so this work explores a simpler alternative in which an acceleration/voltage FRF is used to determine the shaker parameters. When this is done, the results presented here show that multiple sets of shaker parameters can be found that cause the shaker model to match the measured acceleration/voltage FRF, and so a secondary objective is to determine whether each of these solutions will predict the voltage and error in a test with similar accuracy.

This study also presents a simple FRF Multiplication method which can be used to predict test error and shaker voltage without requiring a FEM of the DUT, implementation of dynamic substructuring, or drive point FRF measurements on the DUT. We will compare this method to the substructuring approach and attempt to establish the conditions under which one can expect this simpler procedure to provide reasonable accuracy.

These will be demonstrated using simulation and physical testing on the DUT shown in Figure 3.1. All multiple-input/multiple-output (MIMO) tests in this study were performed using this six shaker setup. Three Siemens Q-Source Miniature Shakers were attached to the bottom of the DUT, exciting in the launch (vertical) direction. Two Modal Shop (MS) K2007E01 Shakers excited the DUT radially, and a Ling Dynamics (LDS) v200 Series Shaker excited in the spin and radial directions via an angle block.

The DUT is the stool shown in Figure 3.2 which is instrumented with three triaxial accelerometers. Three additional triaxial accelerometers were instrumented on a portion of the next assembly included in the lab test (i.e., plate and interface plate), resulting in 17 channels of environment data available from the boost portion of a sounding rocket flight performed by the Kansas City National Security Campus in 2019. The hardware tested in the lab is the same hardware on which data was collected in flight. The average root-mean-square (RMS) acceleration, or the square root of the sum of the squares of the acceleration values at each time step that data was collected, was 2.48g over the 17 accelerometer channels for the boost portion of the flight. In this study, we aimed to replicate the PSD from 100-2000 Hz, and this frequency content has an average RMS value of 0.09 g. Most of the energy was concentrated below

[31] Mayes *et al.*, "Optimization of Shaker Locations for Multiple Shaker Environmental Testing," 2020.

[40] Fickenwirth *et al.*, "Shaker Capability Estimation Through Experimental Dynamic Substructuring," 2023.

[41] Schultz, "Vibration Test Design with Integrated Shaker Electro-Mechanical Models," 2021.

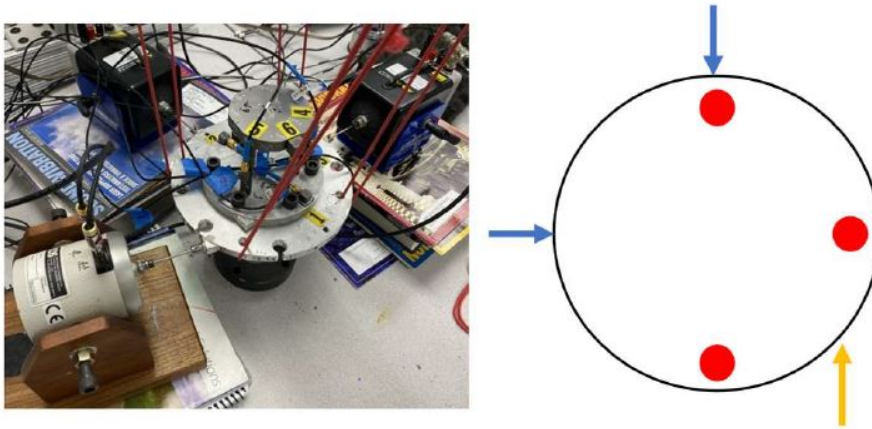


Figure 3.1: Six Shaker MIMO Test Setup (Left) and Schematic Representing Shaker Locations (Right), where the red dots represent Q-Sources on the bottom side of the plate forcing in the launch direction, the yellow arrow represents the LDS shaker forcing in the spin / radial direction, and the blue arrow represents the MS shakers forcing in the radial directions

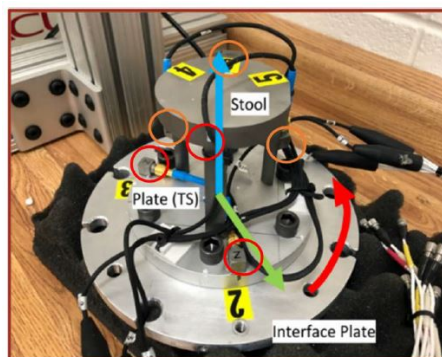


Figure 3.2: Accelerometer Locations on DUT (Orange) and Next Assembly (Red)

100 Hz, hence the disparity between the total RMS acceleration and the RMS acceleration in the frequency band of interest. The Q-Sources cannot force below 50 Hz, and so the 0-100 Hz band was excluded to ensure all shakers functioned properly, while the upper limit was set at 2000 Hz following common practice.

3.2 MIMO Testing Theory

Many forces are exerted on a rocket during flight: thrust, drag, stage separation, and so on. These forces impose stress on each component in the rocket, and the aim of lab qualification tests is to reproduce this vibration induced stress to support design and hardware qualification prior to service. However, it is more practical to compare acceleration in the flight environment and qualification test rather than stress. Stress is correlated to strain, which is determined by the relative displacement at

various points on the DUT, and so acceleration is correlated well to stress if the acceleration response is recreated at a sufficient number of points on the DUT. The forces on the rocket (represented in power spectral density, or PSD, form because of their random nature), $[\mathbf{S}_{FF}(\omega)]$, cause an acceleration response on the DUT, $[\mathbf{S}_{XX}(\omega)]$,

$$[\mathbf{S}_{XX}(\omega)] = [\mathbf{H}_{XF}(\omega)][\mathbf{S}_{FF}(\omega)][\mathbf{H}_{XF}(\omega)]^*, \quad (3.1)$$

where $[\mathbf{H}_{XF}(\omega)]$ is the DUT acceleration/rocket force FRF. In lab MIMO tests, we attach shakers to the DUT, and can solve for the required shaker voltage by inverting the acceleration/voltage FRF,

$$[\mathbf{S}_{VV,LAB}(\omega)] = [\mathbf{H}_{XV}(\omega)]^+ [\mathbf{S}_{XX}(\omega)] [\mathbf{H}_{XV}(\omega)]^{*+}, \quad (3.2)$$

where “+” is the Moore-Penrose pseudoinverse and “*” is the conjugate transpose. This voltage is sent into each shaker resulting in a reconstructed lab environment, $[\mathbf{S}_{XX,LAB}(\omega)]$,

$$[\mathbf{S}_{XX,LAB}(\omega)] = [\mathbf{H}_{XV}(\omega)] [\mathbf{S}_{VV,LAB}(\omega)] [\mathbf{H}_{XV}(\omega)]^*. \quad (3.3)$$

If the error between $[\mathbf{S}_{XX}(\omega)]$ and $[\mathbf{S}_{XX,LAB}(\omega)]$ is small, then the stress the part experiences in flight is assumed to be accurately reconstructed if the DUT is instrumented with enough accelerometers at critical locations.

In a physical MIMO test, the acceleration/voltage FRF is obtained by sending random, uncorrelated voltage signals into each shaker and measuring the response on the DUT. However, at that point significant time and expense has already been invested in the test, so it would be preferable to accurately predict the shaker voltage beforehand. To do so, one must obtain an accurate model of each shaker, a model of the DUT, and then the models must be assembled. This work will demonstrate how to calibrate a basic, lumped-parameter shaker model, and we will then discuss two ways to estimate the shaker voltage required during a MIMO test using this model. First, dynamic substructuring will be used to couple the shaker models to a FEM of the DUT. Second, a novel FRF Multiplication method will be used to estimate this FRF. A summary of both methods is given here, and a theoretical basis for the applicability of the FRF Multiplication method is developed and presented as well.

3.3 Shaker Model Calibration

The parts of a shaker as referenced in this study are labeled in Figure 3.3. Electrodynamical shakers were modeled in this study according to the lumped parameter electromechanical model shown in Figure 3.4. The equations of motion for this system are shown in Equations 3.4 through 3.7,



Figure 3.3: Shaker Body (Red), Armature (Orange), and Calibration Mass (Blue)

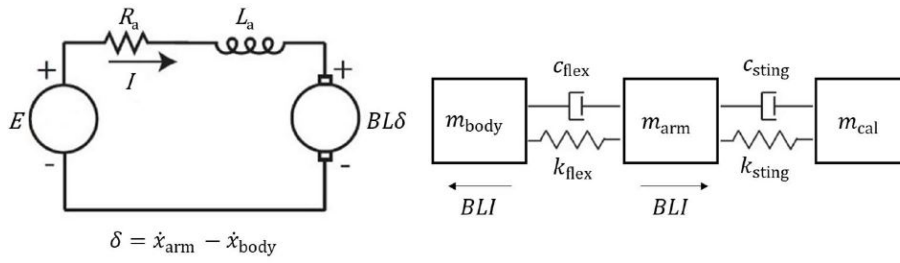


Figure 3.4: Electrodynamic Shaker Model. Left: Electrical Elements. Right: Mechanical Elements.

$$\mathbf{M} = \begin{bmatrix} m_{cal} & 0 & 0 & 0 \\ 0 & m_{arm} & 0 & 0 \\ 0 & 0 & m_{body} & 0 \\ 0 & 0 & 0 & 0 \end{bmatrix}, \quad (3.4)$$

$$\mathbf{C} = \begin{bmatrix} c_{sting} & -c_{sting} & 0 & 0 \\ -c_{sting} & c_{sting} + c_{flex} & -c_{flex} & 0 \\ 0 & -c_{flex} & c_{flex} & 0 \\ 0 & BL & -BL & L_a \end{bmatrix}, \quad (3.5)$$

$$\mathbf{K} = \begin{bmatrix} k_{sting} & -k_{sting} & 0 & 0 \\ -k_{sting} & k_{sting} + k_{flex} & -k_{flex} & -BL \\ 0 & -k_{flex} & k_{flex} & BL \\ 0 & 0 & 0 & R_a \end{bmatrix}, \quad (3.6)$$

$$\mathbf{M} \begin{Bmatrix} \ddot{x}_{cal} \\ \ddot{x}_{arm} \\ \ddot{x}_{body} \\ \dot{I} \end{Bmatrix} + \mathbf{C} \begin{Bmatrix} \dot{x}_{cal} \\ \dot{x}_{arm} \\ \dot{x}_{body} \\ \dot{I} \end{Bmatrix} + \mathbf{K} \begin{Bmatrix} x_{cal} \\ x_{arm} \\ x_{body} \\ I \end{Bmatrix} = \begin{Bmatrix} f_{cal} \\ f_{arm} \\ f_{body} \\ E \end{Bmatrix}, \quad (3.7)$$

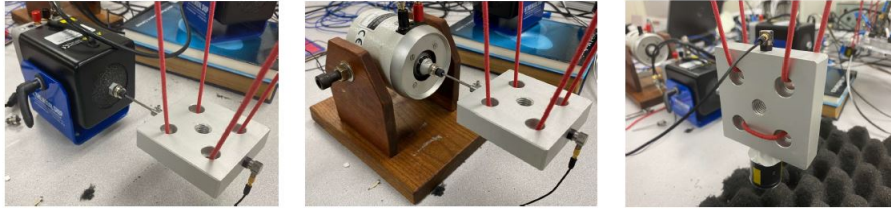


Figure 3.5: Calibration Test Setups for MS (Left), LDS (Center), and Q-Source Shakers (Right)

where the shaker voltage, E , is the input to the system, and shaker current, I , and displacements of the masses are the output variables. The electrical and mechanical portions of the shaker are coupled in two ways: the shaker current induces a force on the armature and shaker body, and a back electromotive voltage is induced in the shaker as the armature moves.

A variation to the common model is to include rotational degrees of freedom which are excited in shaker tables [42], but stingers isolate most of the lateral DUT motion from the armature making this addition unnecessary here. FRF based models are also preferred in some applications as they do not require identifying shaker parameters and can be used to accurately predict certain output variables [43], though a parameter based model was employed here. Some of these model parameters can be measured or obtained from a data sheet, but others must be determined experimentally. Typically, the unknown electrical parameters are armature coil inductance L_a , the product of magnetic flux density and coil length, BL , which is referred to as the back-EMF constant going forward, and possibly resistance, R_a . The unknown mechanical parameters are typically stinger stiffness, k_{sting} , stinger damping, c_{sting} , flexure damping, c_{flex} , and sometimes flexure stiffness, k_{flex} .

A common experimental calibration test is to input random excitation to a shaker and measure the response of a calibration mass as well as the voltage and current in the shaker [44]. Current transducers were not available for this study, so we followed a similar procedure only utilizing voltage measurements. The calibration setups used in this study are shown in Figure 3.5; the MS and LDS shakers were attached to a 0.275 kg mass via a 5 cm stinger, and a uniaxial accelerometer was placed on the side of the mass opposite the shaker. This accelerometer could also have been placed at the drive point, though it was placed on the opposite side for ease of test setup. The Q-Source was attached directly to the mass and was oriented vertically. A 100 mV random signal from 100-4000 Hz was sent into each shaker's amplifier, and the response on the accelerometer was measured. Though multiple MS and Q-Source shakers were used, only one of each was calibrated, and we assumed that the others had the same dynamics.

The voltage input to each shaker, $E(\omega)$, and voltage input to the amplifier, $V_{in}(\omega)$, are related by the amplifier's gain, G_{amp} ,

[42] Hoffait *et al.*, "Virtual shaker testing at V2i: measured-based shaker model and industrial test case," 2016.

[43] Smallwood, "Characterizing Electrodynamic Shakers," 1997.

[44] Schultz, *Calibration of Shaker Electro-mechanical Models*, 2021.

$$E(\omega) = V_{in}(\omega)G_{amp}, \quad (3.8)$$

and the word “voltage” will refer to shaker voltage E going forward (unless otherwise specified) for easier comparison to amplifier output limits. Each shaker’s gain was set to a constant, known value for all tests. The calibration mass was rigid through the testing band, and these tests resulted in an acceleration/voltage FRF for each shaker.

This experimental FRF was compared to the analytical acceleration/voltage FRF obtained using,

$$\{X(\omega)\} = (-\mathbf{M}\omega^2 + \mathbf{C}j\omega + \mathbf{K})^{-1}\{F(\omega)\}, \quad (3.9)$$

and the response of the calibration mass, i.e., the first element of the response vector in,

$$\{X(\omega)\} = \begin{Bmatrix} X_{cal}(\omega) \\ X_{arm}(\omega) \\ X_{body}(\omega) \\ I(\omega) \end{Bmatrix}, \quad (3.10)$$

was calculated to a unit voltage input at each frequency line,

$$\{F(\omega)\} = \begin{Bmatrix} F_{cal}(\omega) \\ F_{arm}(\omega) \\ F_{body}(\omega) \\ E(\omega) \end{Bmatrix} = \begin{Bmatrix} 0 \\ 0 \\ 0 \\ 1 \end{Bmatrix}. \quad (3.11)$$

This FRF was plotted against the experimental one for each shaker in the calibration process. The general calibration process is as follows, and is similar to the process outlined in [44]:

1. Measure parameters that can be measured and obtain all parameters available from shaker data sheets. The calibration mass and the total mass of the shakers are easily measurable. Generally, armature mass and flexure stiffness are specified in the data sheet.
2. Select stinger stiffness and modify flexure stiffness if needed to accurately match the experimental stinger and suspension natural frequencies.
3. Select resistance, inductance, back-EMF constant, and mechanical damping values to match real and imaginary FRF components at and between suspension and stinger natural frequencies.

[44] Schultz, *Calibration of Shaker Electro-mechanical Models*, 2021.

Note that some parameters are measurable or available in the data sheets, but the value measured may not be entirely relevant and so they still must be determined experimentally. For example, the shaker resistance can be measured but it may be temperature dependent or influenced by the amplifier and hence its value was only taken as an initial guess. Step three above is clearly the most difficult, as it involves determining five unknown parameters at the same time. Unfortunately,

these parameters have fairly similar effects on the acceleration/voltage FRF. To illustrate this, these parameters were varied from nominal values, and the effect on the FRF was plotted for the MS shaker in Appendix B.

As seen in Appendix B, the stinger damping predictably damps the stinger mode, while the flexure damping damps the flexure and stinger modes, albeit less significantly than the stinger damping. It is more difficult to describe how the electrical parameters affect the acceleration/voltage FRF; increasing resistance damps the real part of the stinger mode and seems to flatten the curve between flexure and stinger natural frequencies. Increasing inductance damps the real and imaginary parts of the stinger mode, while bringing the magnitude of the real and imaginary parts of both curves closer to zero between natural frequencies. Increasing the back-EMF constant increases the magnitude of the flexure and stinger modes while making these modes more round. Because these parameters affect the acceleration/voltage FRF in similar ways, it is possible to select multiple sets of these parameters that produce a similar FRF. Additionally, the measurements can be expected to include model form errors and noise, so even the best model is not expected to fit the measurements perfectly. Hence, these results suggest that one will not be able to estimate a unique shaker model without measurements of the electrical current, which should remove the ambiguities shown here.

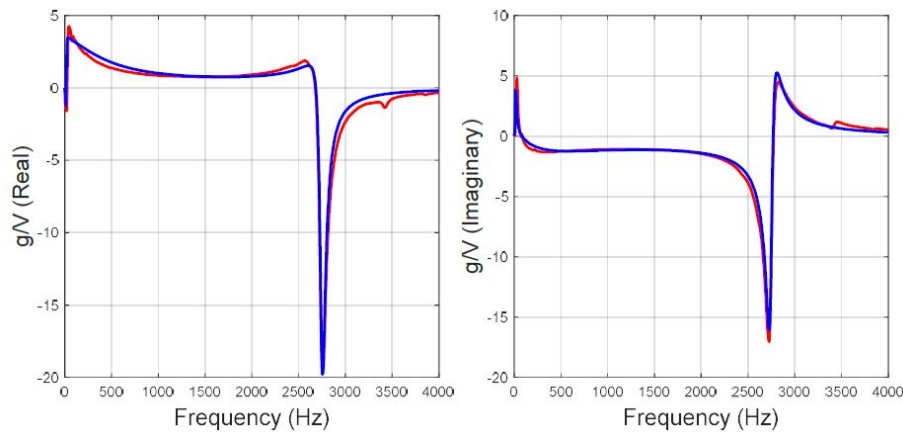
Parameters were selected for each shaker using the previously described procedure, and the best parameters are listed in Table 3.1. One third of the stinger mass was added to the armature and calibration masses to account for the mass coupling between these components. The mass of the adapters connecting the stinger to the armature and the stinger to the calibration mass was also included in the armature and calibration masses, respectively, for the MS and LDS shakers. This was done to account for the mass coupling between the stingers and the calibration mass and armature. The flexure stiffness of the MS and LDS shakers was selected from the data sheet, while the Q-Source's flexure stiffness was varied from the data sheet value to match the experimental FRF better. The stinger stiffness of the MS and LDS shakers was found to be roughly $\frac{3}{4}$ of the analytical axial stiffness. This seems reasonable as the stinger's connections to the armature and calibration mass likely increase the compliance. The Q-Source stinger stiffness was chosen to be large enough that the stinger mode did not appear in the testing band since it is an inertial shaker and is not operated beyond the stinger natural frequency.

The inductance values were all selected as complex numbers to account for inductance losses at high frequencies due to eddy currents in the magnetic pole structure [45]. Interestingly, the stinger damping values differ significantly between the MS and LDS shakers. This is likely because, as shown in the Appendix, resistance and inductance have a damping effect on the FRF. The MS shakers' electrical parameters are all smaller in magnitude than those of the LDS shaker, meaning that most of the FRF's damping is accounted for in its stinger damping term, hence the disparity. For each shaker, the real and imaginary parts of

[45] Dal Borgo *et al.*, "Identification and analysis of nonlinear dynamics of inertial actuators," 2019.

Table 3.1: Parameters Obtained for Each Shaker in the Calibration Process

Parameter Name (Unit)	MS Parameter Value	LDS Parameter Value	Q-Source Parameter Value
Calibration Mass (kg)	0.283	0.283	0.275
Armature Mass (kg)	0.053	0.028	0.01
Shaker Mass (kg)	2.84	2.41	0.09
Flexure Stiffness (N/m)	2630	3500	1.5e5
Stinger Stiffness (N/m)	1.33e7	1.33e7	1e10
Back-EMF Constant (N/A)	2.2	8.4	8
Resistance (Ohm)	0.2	1.5	15
Inductance (H)	(6-2i)*1e-5	(2-i)*1e-4	(9-5i)*1e-4
Flexure Damping (Ns/m)	0.4	0.4	46
Stinger Damping (Ns/m)	19	0.8	1.5

**Figure 3.6:** Experimental (Red) and Analytical (Blue) Acceleration/Voltage FRFs for MS Shakers

the experimental and model FRFs are shown in Figures 3.6 through 3.8. An excellent match was obtained for the LDS and MS shakers, while a reasonable match was obtained for the Q-Sources. These plots suggest that the parameters selected in the calibration process accurately capture the relationship between voltage and acceleration for each shaker.

Similar studies (e.g., [31, 40, 41]) have also used current-based FRFs in the calibration process. An advantage is that the electrical impedance (i.e., voltage/current) FRF makes choosing resistance and inductance more intuitive [44]. While FRFs referencing voltage include electro-

[31] Mayes *et al.*, "Optimization of Shaker Locations for Multiple Shaker Environmental Testing," 2020.

[40] Fickenwirth *et al.*, "Shaker Capability Estimation Through Experimental Dynamic Substructuring," 2023.

[41] Schultz, "Vibration Test Design with Integrated Shaker Electro-Mechanical Models," 2021.

[44] Schultz, *Calibration of Shaker Electro-mechanical Models*, 2021.

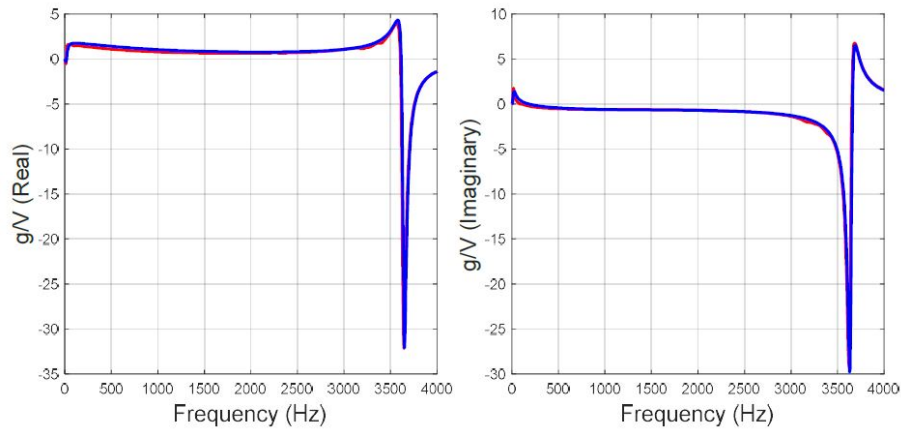


Figure 3.7: Experimental (Red) and Analytical (Blue) Acceleration/Voltage FRFs for LDS Shaker

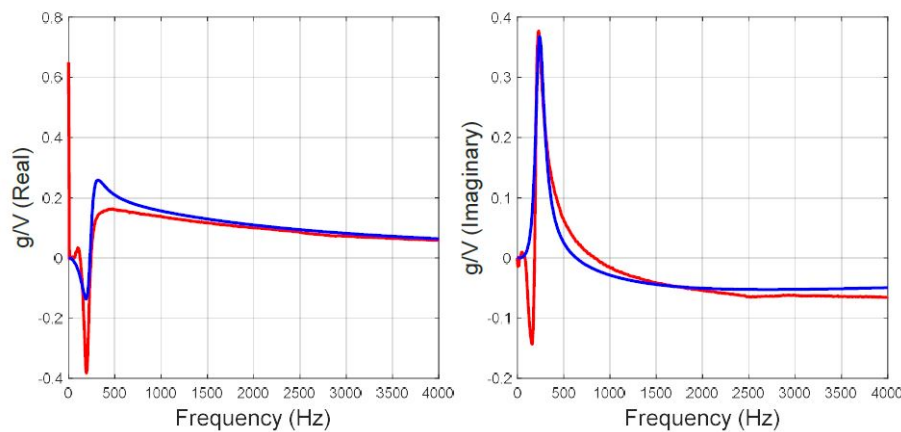


Figure 3.8: Experimental (Red) and Analytical (Blue) Acceleration/Voltage FRFs for Q-Source Shakers

magnetic and structural damping terms, those referencing current only include structural terms, also making it easier to distinguish between unknown electrical and mechanical parameters [39]. Hence, it is more difficult to determine a unique set of shaker parameters with only voltage measurements available, and multiple sets of reasonable parameters could be obtained. A later section addresses whether multiple of these sets yields similar voltage predictions.

3.4 Dynamic Substructuring Theory

Shaker voltage and MIMO reconstruction error were first predicted using dynamic substructuring and then the simplified FRF Multiplication procedure. Substructuring has been implemented for this purpose in previous studies. Component mode synthesis was implemented here because a FEM of the component was available [31]. A brief summary of

[39] Lang *et al.*, "Understanding the Physics of Electrodynamic Shaker Performance," 2001.

[31] Mayes *et al.*, "Optimization of Shaker Locations for Multiple Shaker Environmental Testing," 2020.

the method is given here, though a more detailed description is given in [46].

Substructures were first assembled in block diagonal mass, damping, and stiffness matrices. In this study, there are 13 substructures: the DUT, the six shaker models (Fig. 3.4), and six calibration masses that are subtracted from each shaker model. Since FEMs often have thousands or more degrees of freedom, it is more tractable to use the modal mass, damping, and stiffness matrices for the DUT and to use physical coordinates for the shaker models and calibration masses. Enough modes should be included in these matrices to accurately capture the part's dynamics within the testing band; generally, including modes up to 1.5x the max frequency of interest is sufficient.

Equations of motion of the uncoupled systems can be written as,

$$\begin{bmatrix} \mathbf{M}_{DUT} & 0 \\ 0 & \mathbf{M}_2 \end{bmatrix} \begin{Bmatrix} \ddot{q} \\ \ddot{u}_2 \end{Bmatrix} + \begin{bmatrix} \mathbf{C}_{DUT} & 0 \\ 0 & \mathbf{C}_2 \end{bmatrix} \begin{Bmatrix} \dot{q} \\ \dot{u}_2 \end{Bmatrix} + \begin{bmatrix} \mathbf{K}_{DUT} & 0 \\ 0 & \mathbf{K}_2 \end{bmatrix} \begin{Bmatrix} q \\ u_2 \end{Bmatrix} = [\Phi]^T \{f\} + [\Phi]^T \{g\}, \quad (3.12)$$

where $[\mathbf{M}_{DUT}]$, $[\mathbf{C}_{DUT}]$, $[\mathbf{K}_{DUT}]$ are the modal mass, damping, and stiffness matrices of the DUT, $[\mathbf{M}_2]$, $[\mathbf{C}_2]$, $[\mathbf{K}_2]$ are block diagonal and contain the mass, damping, and stiffness matrices of the shakers and calibration masses (stiffness and damping of calibration masses equals zero), and $[\Phi]$ is block diagonal with the first block containing the mode shapes of the DUT and the second block being the identity matrix. $[\mathbf{M}_2]$, in this case, is 30x30, with the first 24 rows and columns being a block diagonal matrix of each 4 DOF shaker model, and the last 6x6 being a block diagonal containing the negative calibration masses. The calibration mass is subtracted from each shaker model so that the stinger attaches directly to the DUT, mimicking the physical test setup. The right side of the equation includes external applied forces $\{f\}$ and connection forces $\{g\}$ that are nonzero for the degrees of freedom that will be coupled in the substructuring process.

In Eq. 3.12, the DUT and shakers are not yet connected to one another. To enforce this connection, one must define the compatibility matrix, $[\mathbf{B}]$, and a force equilibrium matrix, $[\mathbf{L}]$, as detailed in [46]. The matrix $[\mathbf{B}]$ contains one row for each compatibility constraint, with a 1 and -1 placed at the locations of the degrees of freedom being coupled, resulting in the set of constraints,

$$[\mathbf{B}]\{u\} = \{0\}, \quad (3.13)$$

where $\{u\}$ represents the physical degrees of freedom of all systems $\{u\} = [\{u_{DUT}\}^T \{u_2\}^T]^T$. In the case of interest in this work, $\{u_{DUT}\}$ contains the six locations in which shakers will be connected, as well as 18 accelerometer degrees of freedom corresponding to triaxial measurements at six locations. Those 24 DOF, plus the 30 DOF in $\{u_2\}$ dictate the matrix $[\mathbf{B}]$ have 54 columns. The matrix $[\mathbf{B}]$ has 12 rows here,

[46] Klerk *et al.*, "General Framework for Dynamic Substructuring," 2008.

[46] Klerk *et al.*, "General Framework for Dynamic Substructuring," 2008.

corresponding to six constraints that tie the end of each shaker model calibration mass to a negative calibration mass, and six constraints that tie the negative calibration masses to the shaker's location on the DUT. The physical coordinates are related to the modal coordinates $\{q\}$ of the DUT through the $[\Phi]$ matrix, so the constraints are actually written as,

$$[\mathbf{B}][\Phi] \begin{Bmatrix} q \\ u_2 \end{Bmatrix} = \{0\}, \quad (3.14)$$

showing that the $[\mathbf{B}]$ matrix in the modal coordinate system, $[\mathbf{B}_{CMS}] = [\mathbf{B}][\Phi]$. The force equilibrium matrix, $[\mathbf{L}]$, can be assembled manually by placing a 1 in every row at the appropriate degree of freedom for each degree of freedom that is not coupled to another substructure, and two 1's in a row for each set of degrees of freedom that is being coupled. It can also be solved for as the null space of the $[\mathbf{B}]$ matrix as,

$$[\mathbf{L}_{CMS}] = null([\mathbf{B}_{CMS}]). \quad (3.15)$$

After obtaining $[\mathbf{B}_{CMS}]$ and $[\mathbf{L}_{CMS}]$, the coordinate transformation,

$$\begin{Bmatrix} q \\ u_2 \end{Bmatrix} = [\mathbf{L}_{CMS}]\{\eta\}, \quad (3.16)$$

where $\{\eta\}$ includes only a single degree of freedom for each interface, is applied to the uncoupled equations of motion in Eq. 3.12. This equation is then pre-multiplied by $[\mathbf{L}_{CMS}]^T$ to eliminate the connection forces, resulting in the coupled equation of motion,

$$[\mathbf{M}_{CMS}]\{\ddot{\eta}\} + [\mathbf{C}_{CMS}]\{\dot{\eta}\} + [\mathbf{K}_{CMS}]\{\eta\} = [\mathbf{L}_{CMS}]^T[\Phi]^T\{f\}. \quad (3.17)$$

The acceleration/voltage FRF used to simulate the test is obtained by taking the Fourier transform of Eq. 3.17 and solving for the matrix relating $\{\eta(\omega)\}$ to $\{f(\omega)\}$,

$$\{\eta(\omega)\} = (-[\mathbf{M}_{CMS}]\omega^2 + [\mathbf{C}_{CMS}]i\omega + [\mathbf{K}_{CMS}])^{-1}[\mathbf{L}_{CMS}]^T[\Phi]^T\{f(\omega)\}. \quad (3.18)$$

The response can then be converted to physical coordinates using the modal and primal formulation transformations,

$$\{u(\omega)\} = [\Phi][\mathbf{L}_{CMS}]\{\eta(\omega)\}, \quad (3.19)$$

rendering the FRF in a form that can be used to simulate the test. The substructuring approach that was used here required that we have a modal model of the DUT, which is easy to obtain from a FEM. In practice, it may be more convenient to measure the frequency response functions relating input forces on the DUT to accelerations at specific points. If a matrix of these FRFs were available, the same process could be used to assemble them to the shakers to create the desired acceleration/voltage FRFs that are needed for the MIMO simulations. The equations for implementing this Frequency Based Substructuring (FBS) approach are given in the next section.

3.5 FRF Multiplication Theory

The proposed FRF Multiplication method aims to approximate the substructuring process by multiplying two FRFs: $[\mathbf{H}_{XF}(\omega)]$, which relates force applied to the DUT at shaker locations to acceleration on the DUT at accelerometer locations, and $[\mathbf{H}_{FE}(\omega)]$, which relates the shaker voltage to the force in the stinger. This returns an acceleration over voltage FRF, $[\mathbf{H}_{XE}(\omega)]$,

$$[\mathbf{H}_{XE}(\omega)] = [\mathbf{H}_{XF}(\omega)][\mathbf{H}_{FE}(\omega)]. \quad (3.20)$$

The stinger force is calculated as follows,

$$F_{sting}(\omega) = k_{sting}[X_{cal}(\omega) - X_{arm}(\omega)] + c_{sting}i\omega[X_{cal}(\omega) - X_{arm}(\omega)], \quad (3.21)$$

where $X_{cal}(\omega)$ and $X_{arm}(\omega)$ are calculated by applying a unit voltage input in Eq. 3.9. The acceleration/voltage FRF is accurately obtained if the stinger force, $F_{sting}(\omega)$, is equal to the force applied to the DUT at the shaker location, $F_{sh}(\omega)$, as these terms would cancel as seen in,

$$\frac{X_{acc}(\omega)}{E(\omega)} = \frac{X_{acc}(\omega)}{F_{sh}(\omega)} \frac{F_{sting}(\omega)}{E(\omega)}. \quad (3.22)$$

When shakers are attached to the actual DUT, $F_{sting}(\omega) = F_{sh}(\omega)$, so the acceleration/voltage FRF measured in that test would be accurately replicated using Eq. 3.22. However, it would be more useful to obtain the stinger force/voltage FRF prior to assembling the hardware for the qualification test. For example, it can be measured from the FRFs used in the shaker calibration tests, where masses were connected to the shakers. When this FRF is obtained from the calibration model, however, there is error as force equilibrium and compatibility between the stingers and DUT are not directly enforced.

To understand the difference between the proposed method and existing approaches, a single shaker is coupled to the DUT using the FBS approach, yielding the acceleration/voltage FRF,

$$\frac{X_{acc}(\omega)}{E(\omega)} = \frac{\frac{X_{acc}(\omega)}{F_{sh}(\omega)}}{\frac{X_{sh}(\omega)}{F_{sh}(\omega)} + \frac{X_{cal}(\omega)}{F_{cal}(\omega)}} \frac{X_{cal}(\omega)}{E(\omega)}. \quad (3.23)$$

While Component Mode Synthesis is implemented in the experimental portion of this study, the comparison between FRF Multiplication and FBS is more direct and insightful.

As seen in Eq. 3.23, FBS requires drive point FRFs at the shaker location on the DUT and on the calibration mass in the shaker model. An advantage of the FRF Multiplication procedure, therefore, is that these drive point FRFs, which can require significant effort to obtain, are not required. Hence, a model of the coupled shaker-DUT system can be obtained with less testing. This issue is circumvented in this

work by using a FEM for the DUT, as the mass-normalized mode vectors can be readily obtained from it. In this case, FRF Multiplication is still easier to implement as the compatibility and force equilibrium matrices do not need to be defined and CMS does not need to be performed. In cases where it is a reasonable approximation, it would thus reduce test planning time and cost, making implementation of IMMAT more tractable.

When there are multiple accelerometers on the DUT and multiple shakers, the acceleration/voltage FRFs in the qualification and calibration setups can be written using FBS as,

$$[\mathbf{H}_{X,E}^{DUT+Sh}(\omega)] = [\mathbf{H}_{X,g_2}^{DUT}(\omega)]([\mathbf{H}_{g_2,g_2}^{DUT}(\omega)] + [\mathbf{H}_{g_1,g_1}^{Sh}(\omega)]^{-1}[\mathbf{H}_{g_1,E}^{Sh}(\omega)]), \quad (3.24)$$

$$[\mathbf{H}_{X,E}^{Cal+Sh}(\omega)] = [\mathbf{H}_{X,g_2}^{Cal}(\omega)]([\mathbf{H}_{g_2,g_2}^{Cal}(\omega)] + [\mathbf{H}_{g_1,g_1}^{Sh}(\omega)]^{-1}[\mathbf{H}_{g_1,E}^{Sh}(\omega)]), \quad (3.25)$$

where g_2 are the interface degrees of freedom on the DUT or calibration mass, and g_1 are the interface degrees of freedom at the end of each shaker. Since $[\mathbf{H}_{X,g_2}^{DUT}(\omega)]$ is known from a modal test or FEM of the DUT and $[\mathbf{H}_{g_1,E}^{Sh}(\omega)]$ is an unchanging property of the shakers used in the test, the condition for FRF Multiplication's success can be written succinctly as,

$$([\mathbf{H}_{g_2,g_2}^{DUT}(\omega)] + [\mathbf{H}_{g_1,g_1}^{Sh}(\omega)]^{-1})^{-1} \sim ([\mathbf{H}_{g_2,g_2}^{Cal}(\omega)] + [\mathbf{H}_{g_1,g_1}^{Sh}(\omega)]^{-1})^{-1}. \quad (3.26)$$

These terms will be similar when $[\mathbf{H}_{g_2,g_2}^{DUT}(\omega)]$ and $[\mathbf{H}_{g_2,g_2}^{Cal}(\omega)]$ are much smaller than $[\mathbf{H}_{g_1,g_1}^{Sh}(\omega)]$ as the inverse of the sum of a small and a large number is similar to the inverse of the large number. $[\mathbf{H}_{g_1,g_1}^{Sh}(\omega)]$ relates acceleration and force at the end of the stinger when it is attached to the shaker armature, and so this term is large when the armature is light. (Recall that an acceleration FRF scales as the inverse of the mass.) If the effective mass of the DUT and Calibration mass are large, then those terms will not contribute much to the sum. The case studies in the following section help illustrate this.

3.6 FRF Multiplication Case Studies

A few case studies are presented here to understand when the FRF Multiplication is a reasonable approximation. The method was tested on the simplest analytical systems that are relevant to real applications; the calibration test setup is shown in Figure 3.9, and the electrical circuit, shaker body, and flexure spring were eliminated from the model for the sake of simplicity.

A simple DUT, shown in Figure 3.10, connects two masses via a spring to introduce an elastic mode.

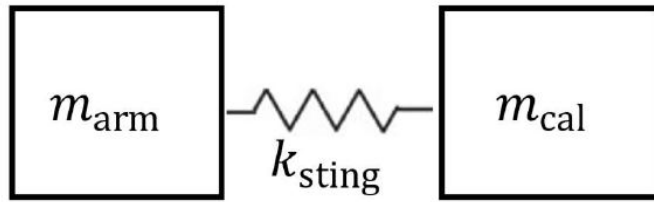


Figure 3.9: Calibration Setup for Case Study

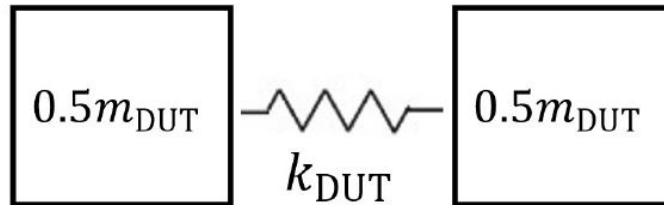


Figure 3.10: DUT for Case Study

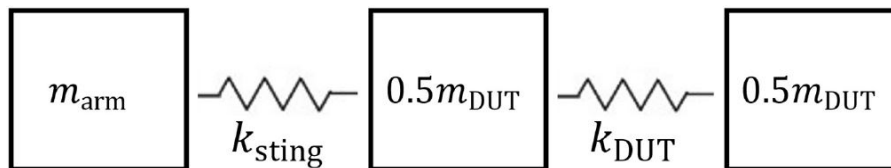


Figure 3.11: Qualification Setup for Case Study

A simple qualification setup couples shaker and component dynamics and is shown in Figure 3.11. The parameter values used in this case study are listed and justified in Table 3.2.

First, we present a case study where a qualification test was simulated to show how error in the estimated FRF affects RMS force predictions. Then, parameters were varied to understand how FRF Multiplication might perform in general. For the first case study, a qualification test was simulated on the system in Fig. 3.11. A simulated environment was obtained using the flight setup in Figure 3.12, where m_{vehicle} is 100 kg and k_{vehicle} was selected to be 1.33e6 N/m to simulate an impedance

Table 3.2: Case Study Parameter Values

Parameter Name (Unit)	Parameter Value	Reason for Value
Armature Mass (kg)	0.053	MS Shaker Value
DUT Mass (kg)	-	Varied to Show Effect
Stinger Stiffness (N/m)	1.33e7	MS Shaker Value
DUT Stiffness (N/m)	-	Varied to Show Effect
Stinger Damping (Ns/m)	10	Arbitrary
DUT Damping (Ns/m)	10	Arbitrary

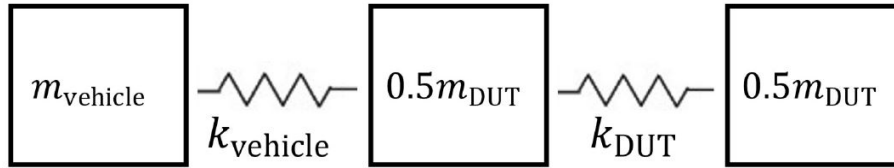


Figure 3.12: Flight Setup for Case Study

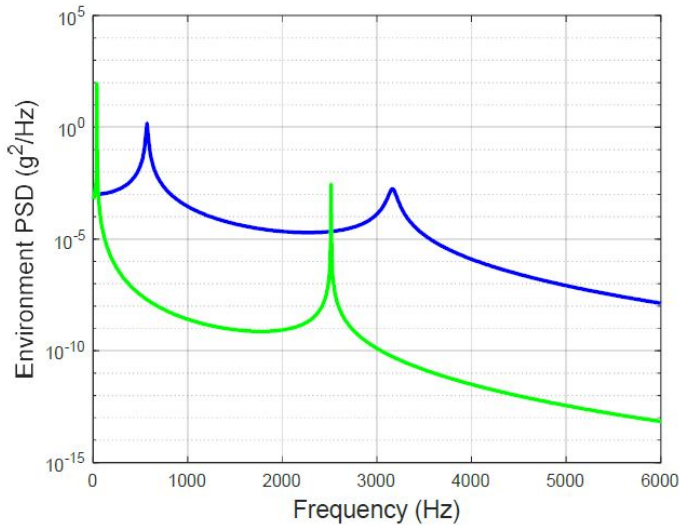


Figure 3.13: Simulated Environments for 0.1 kg DUT (Blue) and 25 kg DUT (Green)

mismatch between the flight and lab test.

A unit force, flat to 6000 Hz, was applied to the vehicle in Fig. 3.12, and the response on the right DUT mass was calculated and converted to a PSD to obtain the flight environments in Figure 3.13. The test was then simulated using Eqs. 3.1 through 3.3 using a DUT acceleration/armature force FRF obtained first using dynamic substructuring and then FRF Multiplication. Armature force was used to represent required shaker effort here as electrical parameters are omitted. Also, both environments were reconstructed with no error because the number of responses being reconstructed equals the number of forces applied, so plots of the reconstructed environment are not shown. In all cases, the calibration mass and DUT mass were the same, though this does not generally need to be the case for reasons explained later.

The armature force auto spectra are shown in Figure 3.14. They show that the forces estimated by the FRF multiplication method were generally accurate, except in a frequency range that is centered on the resonances that occur between 2 and 4kHz in Figure 3.13. The reason for these discrepancies will be explained in the results that follow. First, the RMS force predictions are examined in Table 3.3. There is 1.2% error between the estimates for the small DUT mass and no noticeable error for the larger mass. Since the RMS of a data set heavily weights larger values, the differences between force auto spectra, which occur at low

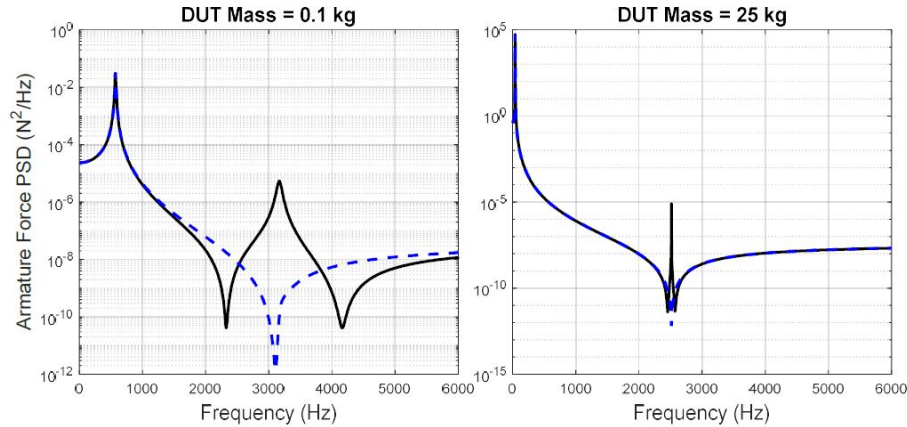


Figure 3.14: Force Auto Spectra: Truth (Black) and Estimate Obtained Using FRF Multiplication (Blue)

Table 3.3: RMS Force (N) Estimates for Simulated Case Study Tests

FRF Estimation Method	$m_{DUT}=0.1$ kg	$m_{DUT}=25$ kg
Substructuring	0.856	108.56
FRF Multiplication	0.867	108.56

force levels here, were minimized, and RMS estimates were very similar even though the spectra are visibly different. If these errors occurred at a frequency where the required force was larger, then the RMS values would be affected much more significantly.

The results shown previously, in which the force predictions were only inaccurate in a small frequency range, can be explained based on the theory in the previous section. Substructuring enforces force equilibrium and displacement compatibility at the connection between the shaker and DUT, while the FRF multiplication method does not but assumes that the dynamics are unchanged from the calibration setup, where the shaker is attached to a rigid mass (e.g., Fig. 3.5). Therefore, FRF multiplication will be accurate if the FRF between the stinger force to the shaker voltage is similar between the calibration (Fig. 3.9) and qualification (Fig. 3.11) setups. These FRFs can be compared for the simple model, with various values of the system's stiffnesses and masses, to understand the conditions under which they differ. To obtain these FRFs, the force between the DUT and armature was found using Eq. 3.21, from the stinger deflection or the difference between the displacement of the DUT and armature.

The uncoupled DUT and stinger each have one mode in this case study, and the results are expected to be most affected when those modes are close so that they interact the most. Hence, the first case considered is one in which the natural frequency of the calibration setup, $\omega_{n,cal}$, equals the natural frequency of the DUT, $\omega_{n,DUT}$. The stinger force / armature force FRFs for the calibration and qualification systems are plotted for two different DUT masses in Figure 3.15. In both cases, the

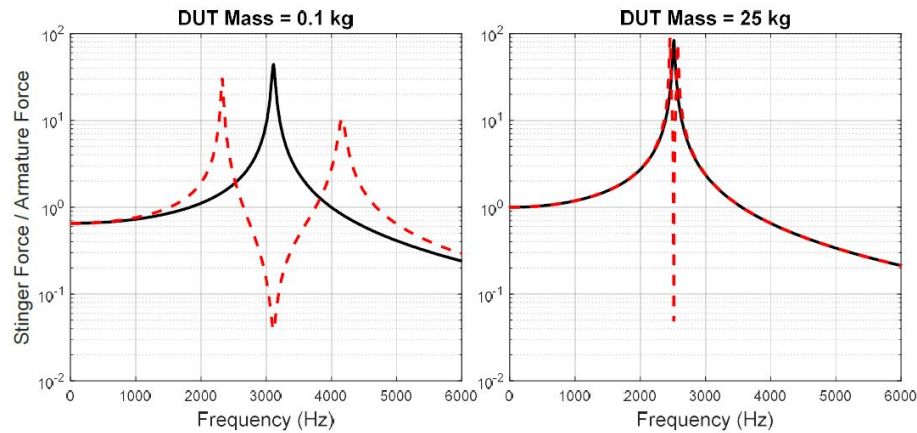


Figure 3.15: Stinger Force/Armature Force FRF for Calibration (Black) and Qualification (Red) Systems with $m_{DUT} = 0.1$ kg and $m_{DUT} = 25$ kg. $\omega_{n,cal} = \omega_{n,DUT}$

natural frequency of the calibration system occurs at the anti-resonance of the qualification system, resulting in error between the two FRFs. The error is mitigated when the DUT mass is larger, as the larger mass causes the natural frequencies and the anti-resonance to move closer together.

To explore what happens when the DUT and calibration systems have different natural frequencies, the case for $\omega_{n,DUT} = 0.5\omega_{n,cal}$ is shown in Figure 3.16. The calibration and qualification FRFs match more closely in this case as the stinger mode in the qualification setup is closer to the stinger mode in the calibration setup and because the anti-resonance of the qualification system no longer lines up with the calibration setup's stinger mode. Still, there is significant error between the FRFs when DUT mass is small. When DUT mass is large, there is again excellent agreement between the FRFs as the DUT mode and anti-resonance of the qualification setup are very narrow and the stinger natural frequency is the same in both setups. Hence, FRF Multiplication is also expected to be more accurate when $\omega_{n,DUT}$ and $\omega_{n,cal}$ are further away from each other.

Since some of the error between calibration and qualification FRFs is concentrated around the calibration setup stinger mode, there would be less error in the approximation if this mode occurred above the highest test frequency as in Figure 3.17. When this is the case, there is still disagreement between the FRFs at the DUT mode and at the anti-resonance of the qualification system, but the error between the stinger modes in the two setups is removed, resulting in a more reasonable approximation. Though the calibration FRF generally overestimates the magnitude of the qualification FRF when the DUT is light, there is near perfect agreement when the DUT is heavier as previously observed. In short, FRF Multiplication is expected to be accurate for this simple case study when m_{DUT} and m_{cal} are large, and it also helps if the stinger mode occurs above the frequency band and if DUT natural frequencies are far away from the stinger natural frequency in the calibration setup.

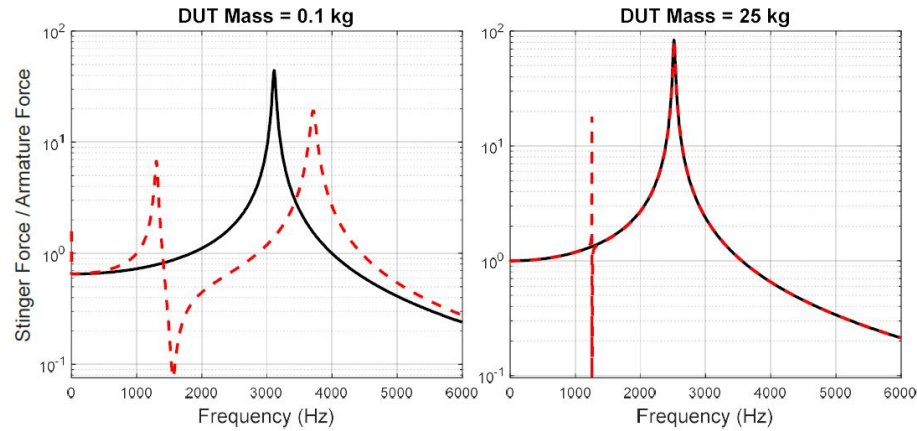


Figure 3.16: Stinger Force / Armature Force FRF for Calibration (Black) and Qualification (Red) Systems with $m_{DUT} = 0.1$ kg and $m_{DUT} = 25$ kg. $\omega_{n,DUT} = 0.5\omega_{n,cal}$

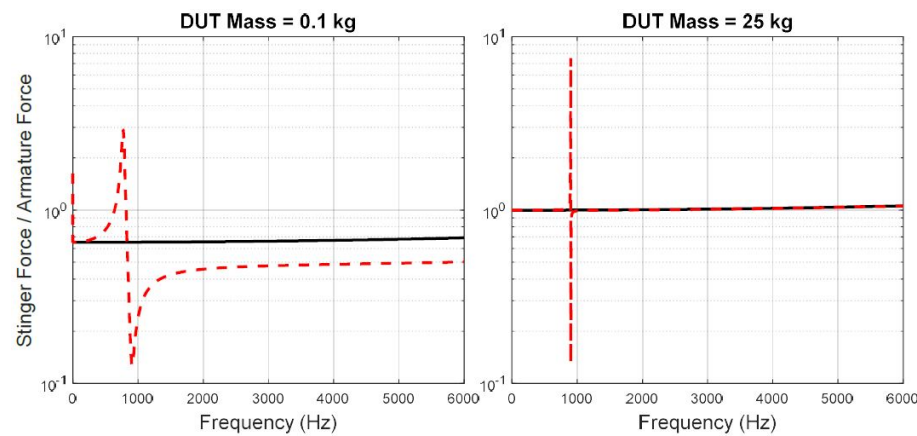


Figure 3.17: Stinger Force / Armature Force FRF for Calibration (Black) and Qualification (Red) Systems with $m_{DUT} = 0.1$ kg and $m_{DUT} = 25$. $f_{n,cal}=25,200$ Hz.(Note the reduced vertical scale relative to the prior figures.)

These observations can also be understood through the lens of vibration absorber theory [47]. In a textbook vibration absorber problem, a single degree of freedom mass-spring system with a natural frequency ω_n is attached to another mass spring system with the same natural frequency, causing the first mass to experience anti-resonance at ω_n in this new two degree of freedom system, which will have one natural frequency above ω_n and one below ω_n . This is essentially what was seen in the first case presented in Fig. 3.15, although all of the systems in this case study are slightly different than the SDOF absorber case, so a brief derivation is presented here.

[47] Rao, *Mechanical vibrations*, 2011.

The FRF relating applied force on the armature, $F_a(\omega)$, to the difference in displacement of the DUT and armature, $Z(\omega) = X_{DUT}(\omega) - X_{arm}(\omega)$, is calculated as,

$$\frac{Z(\omega)}{F_a(\omega)} = \frac{m_{DUT}}{-m_{arm}m_{DUT}\omega^2 + k_{sting}(m_{arm} + m_{DUT})}. \quad (3.27)$$

This system has a single elastic mode at,

$$\omega_{n,cal} = \sqrt{\frac{k_{sting}(m_{arm} + m_{DUT})}{m_{arm}m_{DUT}}}, \quad (3.28)$$

and no anti-resonances, so it is similar to the SDOF unmodified system in the standard vibration absorber problem. The same FRF was calculated for the qualification system, and we find that it has a single anti-resonance at,

$$\omega_{0,qual} = \omega_{n,DUT} = \sqrt{4\frac{k_{DUT}}{m_{DUT}}}, \quad (3.29)$$

which is also the natural frequency of the DUT in Fig. 3.10. When $\omega_{n,cal} = \omega_{n,DUT}$, i.e., when the calibration system natural frequency lines up with the anti-resonance of the qualification system, we see large errors in using the FRF multiplication method, as observed in Figs. 3.15 and 3.16. The qualification system also has two natural frequencies,

$$\omega_{n,qual} = \sqrt{\frac{2m_{arm}(2k_{DUT} + k_{sting}) + k_{sting}m_{DUT} \pm \alpha}{2m_{arm}m_{DUT}}}$$

$$\alpha = \sqrt{8k_{DUT}^2m_{arm}^2\left(2 - \frac{k_{sting}m_{DUT}}{k_{DUT}m_{arm}}\right) + k_{sting}^2(4m_{arm}^2 + 4m_{arm}^2 + 4m_{arm}m_{DUT} + m_{DUT}^2)}. \quad (3.30)$$

If $m_{DUT} \gg m_{arm}$, then $m_{arm} \sim 0$, so $m_{arm} + m_{DUT}$ roughly equals m_{DUT} in the numerators of Eqs. 3.28 and 3.31, and the calibration and qualification systems then have the same natural frequency,

$$\omega_{n,cal} = \omega_{n,qual} = \sqrt{\frac{k_{sting}}{m_{arm}}}. \quad (3.31)$$

This supports the previously observed trend (seen in Figs. 3.15 through 3.17), where the stinger natural frequency was the same in the calibration and qualification FRFs when the DUT mass was large. In other words, there is no significant dynamic interaction between the DUT and shaker models when the DUT mass is much larger than the armature mass, so the calibration and qualification system FRFs are similar.

The equations above explain how the natural frequencies of the calibration and qualification systems differ for this simple case study and help to explain how the dynamics of the shaker and DUT affect the accuracy of the FRFs upon which the FRF multiplication method is based. The results show that the errors tend to be concentrated near the modes of the qualification system, and that in some cases, the differences can be quite small.

The preceding discussion assumes that shakers are attached to a portion of the next assembly that elastically deforms within the test frequency range. This is not uncommon in IMMATs, and elasticity in

[48] Taylor, "Using Transfer Path Analysis and Frequency Based Substructuring To Develop A Robust Vibration Laboratory Dynamic Test Fixture Design Process," 2020.

[49] Schoenherr *et al.*, *Use of Topology Optimization to Design Shock and Vibration Test Fixtures*, 2020.

test fixtures can even be leveraged to more accurately match in flight boundary conditions [48, 49]. However, when shakers are attached to a rigid portion of the next assembly, FRF Multiplication is expected to be a better approximation of the substructuring process because the vibration absorber effect is not observed in this case, so the stinger force/voltage FRF is the same in the calibration and qualification setups.

Returning to the application of interest, where the goal is to predict the shaker voltages as in Figure 3.14, error in an FRF obtained using the multiplication procedure will not cause significant error in RMS force or voltage predictions unless these frequencies occur in a frequency band where the force has significant magnitude. In the prior example, if the environment had more significant acceleration content between 2000 and 4500 Hz, more force would be required between those frequencies, and the RMS force predictions in the small DUT mass case would likely be very inaccurate. The accuracy of the RMS voltage prediction, therefore, is correlated to the accuracy of the multiplied FRF, but it also depends on where shaker energy is required to reconstruct the environment.

In the previous case studies, FRF multiplication was more accurate when the DUT and calibration mass were much larger than the armature mass. For real systems with multiple active modes, it is misleading to state that the DUT mass must be much larger than the armature mass, as the local compliance of the structure matters. If a shaker was attached to a plane's wing, for example, then the drive point effective mass (or force/acceleration FRF) is small even though the mass of the whole plane is large. For real systems, therefore, the effective mass at the drive point of the DUT and calibration mass must be much larger than the drive-point effective mass at the end of the stinger for the stinger-armature system. This is apparent in Eq. 3.26, where the two terms are most similar when the drive point acceleration of the DUT and calibration mass are both small. Hence, this method may not work well when shakers are attached to a point on a massive structure where there is significant local deformation and low effective mass.

To demonstrate this, a single MS shaker model was coupled to the DUT FEM via dynamic substructuring at two points shown in Figure 3.18: first, at the rigid next assembly, and second, at the top of the DUT, where there is a mode around 800 Hz, reducing the drive point effective mass. Both of the shakers were attached to the DUT in the out-of-page direction, which is orthogonal to the motion of the shown mode, but excites a similar mode in the out-of-page direction at the same frequency. The stinger force/voltage FRF was calculated in both cases and compared to the stinger force/voltage FRF determined from the experimental calibration setup. From the previous discussion, we expect that FRF Multiplication can accurately approximate coupled system dynamics when the shaker is attached to the next assembly but not when it is attached to the top of the DUT due to the lower effective mass and vibration absorber effect.

As seen in Figure 3.19, when the shaker is attached to the DUT via the interface plate, which experiences slight elastic deformation at

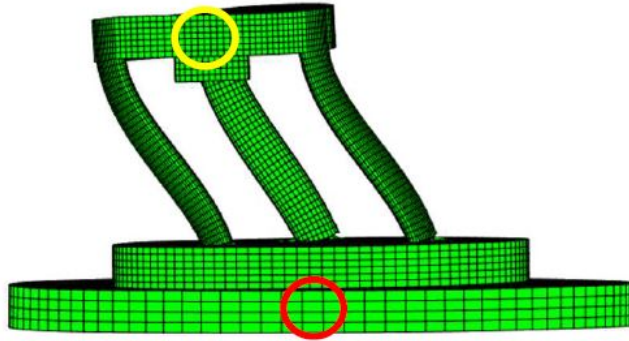


Figure 3.18: Free-Free Bending Mode of DUT, 795 Hz, with Fixture Attachment Location in Red and Stool Attachment Location in Yellow

2650 Hz and is otherwise rigid, the stinger force/voltage FRF from the calibration model (i.e., when a rigid mass is connected to the shaker) very closely matches the FRF from the qualification setup (i.e., when the shaker is connected to the FEM of the DUT using substructuring). When the shaker is attached to the top of the stool, there is a larger discrepancy between the FRFs; the stinger mode is shifted to the right by 100 Hz because of the vibration absorber effect, and there is deviation around 800 Hz due to the decrease in drive point effective mass of the stool at its 800 Hz mode. This seems to confirm the trends seen in the simple case study. Even though there is some error, the calibration FRF still approximates the FRF of the substructured system reasonably well at both attachment locations. This makes sense in light of the theory presented earlier because the calibration model stinger mode occurs at 2550 Hz, which is not very close to the DUT natural frequency, and this reduces the severity of the absorber effect. Also, the effective mass of the top stool configuration is still generally large enough to be represented well by the calibration mass, with deviation at 800 Hz only. Based on these results, we would expect the FRF Multiplication method to work fairly well for either of these test setups.

A summary of the factors that impact FRF Multiplication's accuracy is given in Figure 3.20. In this figure, $m_{eff}(\omega)$ refers to the drive point effective mass of each system. When the effective mass of the DUT and calibration mass are both much larger than that of the stinger-armature system, the terms in Eq. 3.26 are very similar in magnitude. If the drive points are also rigid, then the vibration absorber effect is not observed, and FRF Multiplication is a very good approximation of substructuring. Low effective mass of the calibration mass or DUT results in error in Eq. 3.26 and also amplifies the severity of the absorber effect when shakers are not attached at rigid points. Lastly, the closer the DUT and stinger natural frequencies are, the more severe the absorber effect is, and FRF Multiplication will be less accurate.

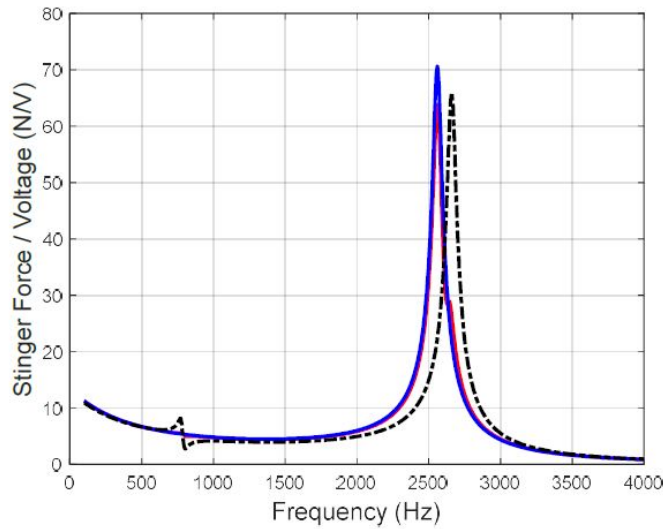


Figure 3.19: Stinger Force/Voltage FRF in Calibrated Shaker Model (Blue) and Substructured Qualification Setup with Shaker Attached to Interface Plate (Red) and Top of Stool (Black)

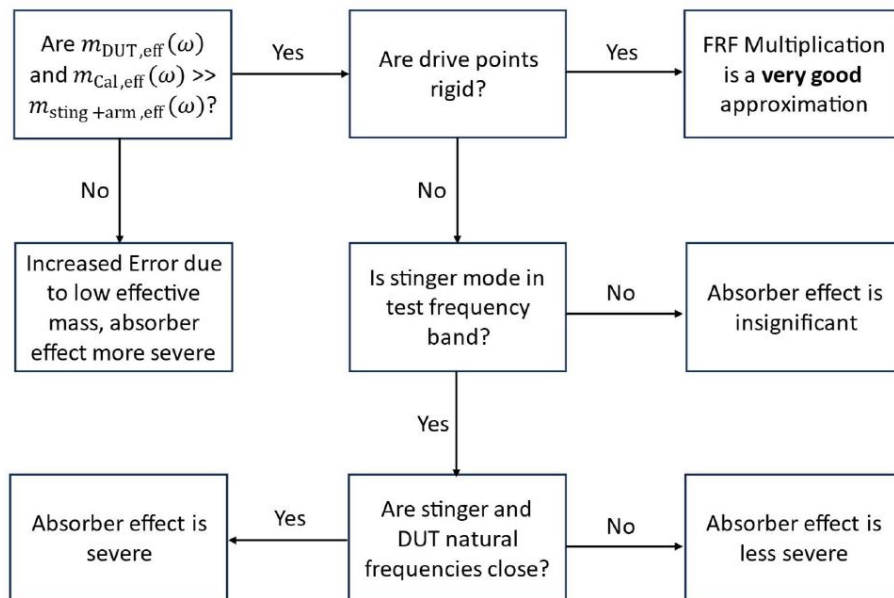


Figure 3.20: Summary of Conditions for Success of FRF Multiplication

Table 3.4: Shaker RMS Force Limits and Amplifier RMS Output Voltage Limits

Shaker Name	RMS Force Limit (lb)	Amplifier Name	RMS Voltage Output Limit (V)
Modal Shop K2007E01	5	SmartAmp 2100E21-100	21
Ling Dynamics v200 Series	« 4	B&K 2706	15
Siemens Q-Source Miniature Shaker	0.45	Siemens Q-Sources Amplifier	31

3.7 Results

Various variables can limit shaker performance including armature displacement and shaker current [39], but we are interested in predicting shaker voltage (i.e., voltage out of the amplifier) in this study. The shaker RMS force limits and amplifier RMS output voltage limits for the shakers used in this study are listed in Table 3.4. For the LDS shaker, the RMS force limit is not specified but is expected to be much less than the sine force limit of 4 lb.

To evaluate the merit of the substructuring and FRF Multiplication methods in predicting test error and shaker voltage, a MIMO test was performed using the setup shown in Fig. 3.1. Though shaker models were calibrated up to 4000 Hz, the MIMO test was performed up to 2000 Hz as the DUT was expected to experience the most significant stress below this frequency. All 17 accelerometer channels in Fig. 3.2, i.e., 5 radial, 6 spin, and 6 launch, were controlled using Eqs. 3.1 through 3.3. The test was simulated using acceleration/voltage FRFs obtained via dynamic substructuring and FRF Multiplication.

In the substructuring case, the shakers were connected to the DUT FEM at the node closest to the point of attachment of each shaker in Fig. 3.1. Compatibility and force equilibrium were enforced in each shaker's direction of excitation. To reduce modal truncation error in the 2000 Hz bandwidth, the DUT's modal model included 20 modes (ranging from 0 to 5520 Hz). The damping ratios of the first three elastic modes were experimentally found to be 0.018, 0.018, and 0.009. These three modes, occurring at 793, 795, and 885 Hz, are the only modes in the 100-2000 Hz band and are thus expected to affect the DUT FRF most significantly in this band. The damping ratios of the remaining 11 elastic modes were assumed to be 0.01. This assumption is not expected to cause significant error as the higher modes have only a small effect on the FRF up to 2000 Hz.

Two sets of simulation results are presented for the FRF Multiplication

[39] Lang *et al.*, "Understanding the Physics of Electrodynamic Shaker Performance," 2001.

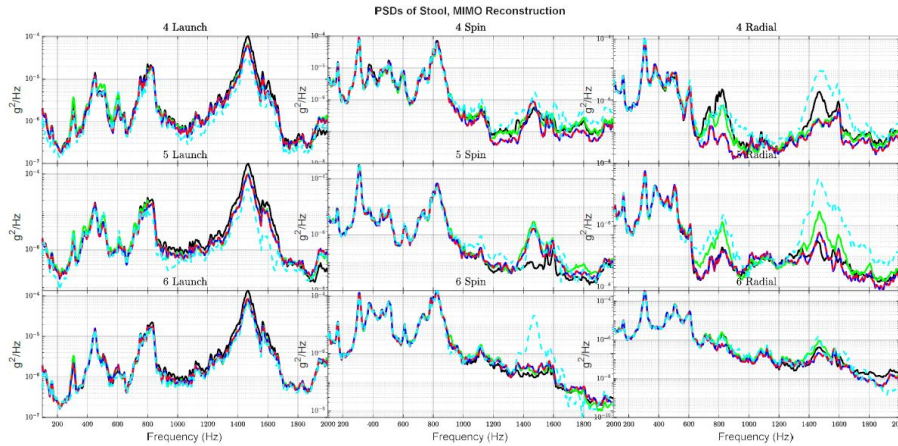


Figure 3.21: Stool Accelerometer PSDs in Launch, Spin, and Radial Directions at Three Locations in the Flight Environment (Black) and MIMO Test (Green), with predictions from Substructuring (Blue), FEM Multiplication (Red), and Roving Hammer Multiplication (Cyan)

method. In both cases, the stinger force/voltage FRF was obtained analytically from each shaker’s calibrated model. For the first set of results, the acceleration/force FRF was obtained from the DUT FEM. This provides the most direct comparison of how closely FRF Multiplication approximates the substructuring process for this DUT. In the second set of results, the acceleration/force FRF was obtained via a roving hammer test on the unit. This will show how accurately voltage can be predicted when a FEM is not available, and the DUT model must instead be obtained experimentally.

The test was simulated using Eqs. 3.1 through 3.3, resulting in the environment reconstruction shown in Figure 3.21. The first three test accelerometers (8 channels) are located on the plate, though these results are not included as the objective is to accurately replicate stress on the DUT, i.e., the stool in Fig. 3.2. Ideally, the MIMO test results would match the flight environment perfectly, though there is least squares error here as there are 6 shakers and 17 controlled channels. In this case, it is hoped that all simulation results would match the MIMO test results exactly so that shaker locations could be accurately selected to reduce reconstruction error, e.g., using the algorithm in [30].

As seen in Fig. 3.21, the simulated environments generally match the MIMO test environments closely. The most significant deviation occurs when the roving hammer FRF is used with the FRF Multiplication procedure. It is uncertain why this is the case, though one possible explanation is that the roving hammer FRF does not account for coupling between shaker inputs, rather assuming that each shaker acts independently. The substructuring and FRF Multiplication on the FEM both predict the test environment reconstruction very accurately with significant deviation only across narrow frequency bands on select channels, e.g., around 800 Hz on the 4th and 5th radial channels. In these two simulations, any

[30] Rohe *et al.*, “Strategies for Shaker Placement for Impedance-Matched Multi-Axis Testing,” 2020.

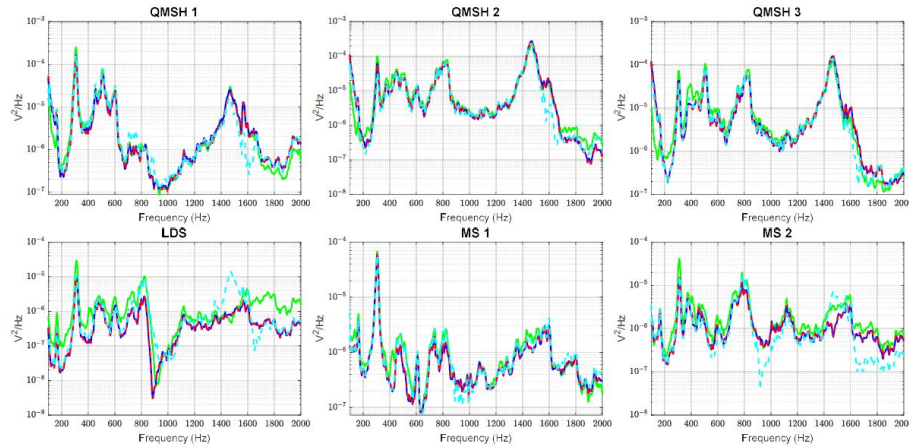


Figure 3.22: Voltage PSDs for MIMO Test (Green), Substructuring (Blue), FRF Multiplication with FEM (Red), and FRF Multiplication with Roving Hammer Measurements (Cyan)

deviation is most likely due to error in modeling the DUT, as error in shaker models should only change the relationship between applied voltage and force while not significantly changing component dynamics.

The Voltage PSDs in the MIMO test and simulations are shown for each shaker in Figure 3.22. Again, the roving hammer FRF used with FRF Multiplication has the most significant disagreement with the MIMO test results, though all simulations generally match the shape of the test PSDs closely. The Q-Sources and MS shakers seem to match particularly well, while there is more significant error in modeling the LDS shaker below 800 Hz and above 1600 Hz in particular. A source of error in these predictions is the FEM of the DUT, as it was a preliminary model and was not updated to match experimental data. There is also some error in the calibrated shaker models, though these errors were shown to be relatively small in Figs. 3.6 – 3.8.

The merit of each simulation can also be compared using the RMS voltage and error values from 100-2000 Hz. The RMS shaker voltage for each simulation was calculated by taking the square root of the area under the voltage PSDs. Reconstruction error was quantified using the RMS dB error metric described in [27]; at each frequency line, the RMS of the difference between the flight and lab environments is taken across all accelerometers, resulting in a dB error value at each frequency line. The RMS of the dB error values is then taken across the frequency lines, resulting in one environment reconstruction error value. The RMS dB error and RMS shaker voltages are compared for the MIMO test, substructuring simulation, and FRF Multiplication simulations in Table 3.5.

As seen in the table, the FRF of the substructured system predicts test RMS voltages closely. As noted earlier, there is the most error in estimating the LDS shaker RMS voltage. Applying FRF Multiplication to the FEM acceleration/force FRF, we obtain RMS voltage predictions

[27] Schumann *et al.*, "Transmission Simulator Based MIMO Response Reconstruction," 2022.

Table 3.5: RMS Shaker Voltage in MIMO Test, Substructured FRF Simulation, and FRF Multiplication Simulations from 100-2000 Hz

Test Metric	MIMO Test	Substructuring	FRF Multiplication - FEM	FRF Multiplication - Roving Hammer
RMS Error (dB)	4.5	4.4	4.4	8.4
V_{RMS} Q-Source 1	1.17	1.05	1.04	1.06
V_{RMS} Q-Source 2	1.78	1.82	1.83	1.69
V_{RMS} Q-Source 3	1.57	1.56	1.58	1.50
V_{RMS} LDS	0.328	0.199	0.193	0.298
V_{RMS} MS 1	0.177	0.151	0.155	0.161
V_{RMS} MS 2	0.218	0.168	0.171	0.180

that are identical to those predicted using the substructuring FRF to the hundredths place. For this system, FRF multiplication is an excellent replacement for substructuring because the next assembly is rigid. When the acceleration/force FRF is obtained from the roving hammer test, there is more deviation from the substructured predictions, though predictions are generally close to the actual test RMS voltage values. All RMS voltage predictions are well within amplifier limits, so each method correctly predicted that this test could be performed successfully.

It is worth noting that the FRF Multiplication method with roving hammer measurements is by far the easiest to implement. The other methods required creating a FEM and using it to extract a modal model for the DUT. Alternatively, one could have measured the drive point FRFs at each shaker attachment point, fit a modal model to the measurements, and then used conventional frequency modal substructuring. That set of measurements could also be used to perform frequency based substructuring. In contrast, the FRF Multiplication method only required the FRFs when a hammer impact is applied at the shaker location, with the response measured at any points of interest.

Both substructuring and the FRF Multiplication - FEM methods estimate MIMO test error very closely. Error prediction was worse when FRF Multiplication was applied to the acceleration/force FRF obtained in the roving hammer test; again, this may be because the forces in the roving hammer test were not applied simultaneously. Some locations on the DUT were also difficult to excite in the correct direction in the roving hammer test, and this could have caused some error as well.

Overall, though, RMS voltage and environment reconstruction error were both predicted with reasonable accuracy using both the substructuring and FRF Multiplication techniques. This agrees with the previously shown theory because the next assembly was rigid in this case and FRF

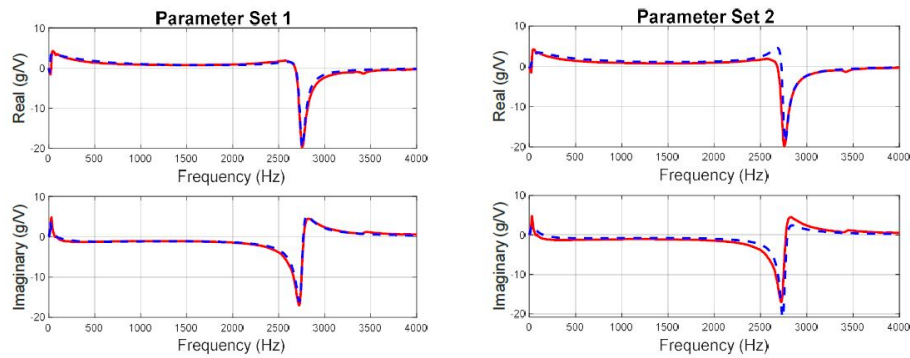


Figure 3.23: Measured (Red) and Model (Blue) Acceleration/Voltage FRFs for First and Second Parameter Sets for the MS Shaker

Multiplication closely approximates the substructuring process here. It is also helpful that roving hammer predictions are reasonable as this procedure is more manageable than obtaining drive point FRFs at each shaker location.

3.8 Uniqueness of Shaker Models

As mentioned previously, it is possible that there are multiple sets of parameters that would match a shaker model to an experimental FRF. This is particularly important in this study, as shaker parameters are selected using an acceleration/voltage FRF and electrical current measurements, which aid in electrical parameter selection [44], are not available.

To evaluate this, two sets of parameters were found that both produced models whose FRFs closely matched those measured for the MS shaker, and these values are shown in Table 3.6. All mass and stiffness values are the same in both sets since these parameters can be measured, obtained from a data sheet, or selected to match natural frequencies to an experimental FRF. The electrical parameters and mechanical damping terms were varied between the parameter sets, as they have similar effects on the acceleration/voltage calibration FRF and hence could be varied without dramatically decreasing the accuracy of the model. The model FRFs are similar for these two sets of parameters, despite this significant change to the parameters, as shown in Figure 3.23.

Though both sets of parameters match the calibration FRF closely, their electrical models are quite different, so it is not clear whether the voltage and error predictions would be significantly different for these sets of shaker parameters. To evaluate this, a six shaker MIMO test was simulated using dynamic substructuring. All shakers were coupled at the same locations, and all of the shaker models were the same except for those for the two MS shakers and the LDS shaker, which was also modeled using a different set of parameters that resulted in a similar FRF as the original calibration. RMS voltage and error predictions for this simulated test are listed in Table 3.7. Q-Source voltage predictions

[44] Schultz, *Calibration of Shaker Electro-mechanical Models*, 2021.

Table 3.6: Two Sets of Parameters Obtained in Calibration for the MS Shaker

Parameter Name	Parameter Value 1	Parameter Value 2	Method of Selection
Calibration Mass (kg)	0.283	0.283	Measurement
Armature Mass (kg)	0.053	0.053	Data Sheet
Shaker Mass (kg)	2.84	2.84	Measurement
Flexure Stiffness (N/m)	2630	2630	Data Sheet
Stinger Stiffness (N/m)	1.33e7	1.33e7	Calibration
Back-EMF Constant (N/Amp)	2.2	5	Calibration
Resistance (Ohm)	0.2	0.37	Calibration
Inductance (H)	6e-5-2e-5i	1e-4-1e-4i	Calibration
Flexure Damping (Ns/m)	0.4	7	Calibration
Stinger Damping (Ns/m)	19	8.5	Calibration

Table 3.7: MIMO Test Simulation with Two Sets of Calibrated Parameters

Test Metric	MIMO Test	Substructuring: Cal 1	Substructuring: Cal 2
Stool Error (dB)	4.5	4.4	4.4
V_{RMS} LDS	0.328	0.199	0.216
V_{RMS} MS 1	0.177	0.151	0.155
V_{RMS} MS 2	0.218	0.168	0.174

are omitted as they are identical in both simulations. As seen in the table, the voltage predictions for the MS and LDS shakers are very similar for both parameter sets. Test error predictions are identical as shaker models do not significantly influence DUT dynamics. It seems, therefore, that the important factor in voltage prediction is only whether the shaker model accurately reproduces the FRF, even if a unique set of mechanical damping and electrical parameters cannot be confidently identified.

It is important to note that when a shaker model is calibrated using the

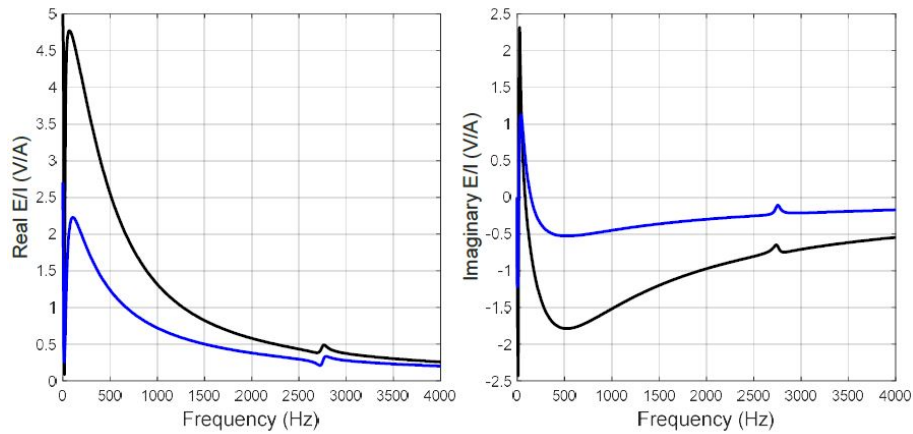


Figure 3.24: MS Electrical Impedance FRFs for Parameter Set 1 (Black) and Parameter Set 2 (Blue)

acceleration/voltage FRF, the model is not necessarily accurate for output variables besides acceleration. This is clearly seen in Figure 3.24, which shows the voltage over current FRFs for the models. The voltages were similar for both models, but these electrical impedance FRFs show that the relationship between voltage and current was significantly different; the current in the shaker differed by a factor of two to three between these models. If an experimental electrical impedance FRF were available, it could be used to determine a unique set of shaker parameters. Then one would expect to be able to predict the shaker current accurately.

3.9 Conclusion

Impedance Matched Multi-Axis Testing is an alternative to single axis testing that can more accurately replicate a component's operational vibration-induced stresses, but increased cost and setup time hinders its implementation. The aim of this chapter was to predict shaker voltage and environment reconstruction error so that the cost and setup time could be reduced, making these tests more manageable.

To this end, dynamic substructuring was used to couple shaker models to a model of the DUT, yielding accurate RMS shaker voltage and environment reconstruction error predictions. FRF Multiplication, which is mathematically simple and requires less information about the DUT's dynamics, was presented as an approximation of the substructuring process, and it was shown to be most accurate when shakers are attached to a rigid next assembly. When the next assembly is not rigid, it was still found to be a reasonable approximation when the DUT is much heavier than shaker armatures. It was found to be a weak approximation when the DUT is light relative to the shakers' armatures, when DUT natural frequencies are close to the stinger natural frequency in the calibration setup, and when shaker stinger modes appear in the qualification test setup. Even so, reasonable RMS shaker voltage estimates were obtained

using an inaccurate FRF because significant shaker force was not required at frequencies where there was the most error. RMS shaker voltage prediction accuracy was, therefore, found to depend on the accuracy of the FRF as well as the specific environment being reproduced.

Shaker models were obtained using an experimentally obtained acceleration/voltage FRF. Flexure and stinger damping as well as coil resistance, inductance, and the back-EMF constant were found to affect this FRF in similar ways and hence proved difficult to uniquely identify. Shaker voltage and test error were accurately predicted when the shaker model FRF closely matched the measured FRF, though, regardless of the specific values of these parameters. Hence, current measurements are only needed if one wishes to accurately estimate the required shaker current.

4

Number of Shakers

This chapter is composed from a paper entitled “Improving IMMAT Planning Through Shaker Modeling and Modal Filtering” presented at the 42nd International Modal Analysis Conference in 2024 [50]. I hereby confirm that the use of this article is compliant with all publishing agreements.

[50] Behling *et al.*, “Improving IMMAT Planning Through Shaker Modeling and Modal Filtering,” 2024.

The thesis author is the primary author of all content in this chapter.

4.1 Modal Filtering

An unanswered question from the previous discussion is how many shakers must be used in an IMMAT to guarantee accurate reconstruction. One way to determine this is to simulate a MIMO test using an increasing number of shakers and stopping when the error is within acceptable limits[30]. Modal filtering can be applied to the same end, yielding improved understanding of the dynamic differences between the flight and lab setups in the process.

[30] Rohe *et al.*, “Strategies for Shaker Placement for Impedance-Matched Multi-Axis Testing,” 2020.

The flight environment measured on the DUT can be described as a linear combination of a set of flight mode shapes,

$$[\mathbf{S}_{XX}(\omega)] = [\Phi_{FLIGHT}][\mathbf{S}_{QQ}(\omega)][\Phi_{FLIGHT}]^*. \quad (4.1)$$

The flight environment can be projected onto a set of lab modes using,

$$[\mathbf{S}_{QQ,EST}(\omega)] = [\Phi_{LAB}]^+[\mathbf{S}_{XX}(\omega)][\Phi_{LAB}]^{*+}, \quad (4.2)$$

and if there are more accelerometer channels than lab modes being projected onto, this will be a least squares projection as lab modes generally do not span the response space of the DUT in flight. The flight environment can then be estimated as a linear combination of lab modal accelerations,

$$[\mathbf{S}_{XX,EST}(\omega)] = [\Phi_{LAB}][\mathbf{S}_{QQ,EST}(\omega)][\Phi_{LAB}]^*. \quad (4.3)$$

We can quantify the differences between the flight and estimated environments using the previously mentioned RMS dB error metric on $[\mathbf{S}_{XX}(\omega)]$ and $[\mathbf{S}_{XX,EST}(\omega)]$. This process can be used to determine what set of lab mode shapes forms a sufficient basis set for the flight environment within the test frequency band, as there would be no error when the lab modes span the space of the flight modes. The modal projection error metric [17]

[17] Schoenherr *et al.*, “Improve Replication of In-service Mechanical Environments.” 2018.

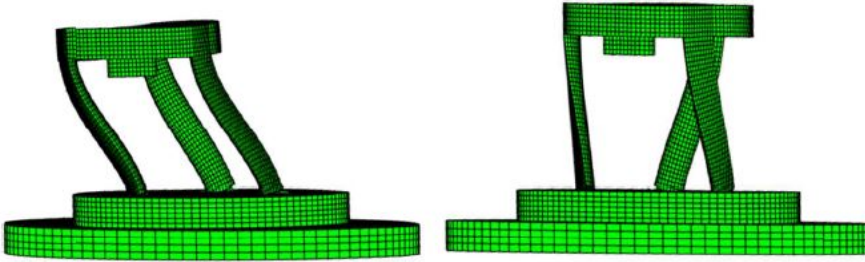


Figure 4.1: First (783 Hz) and Third (885 Hz) Free-Free Mode Shapes of DUT

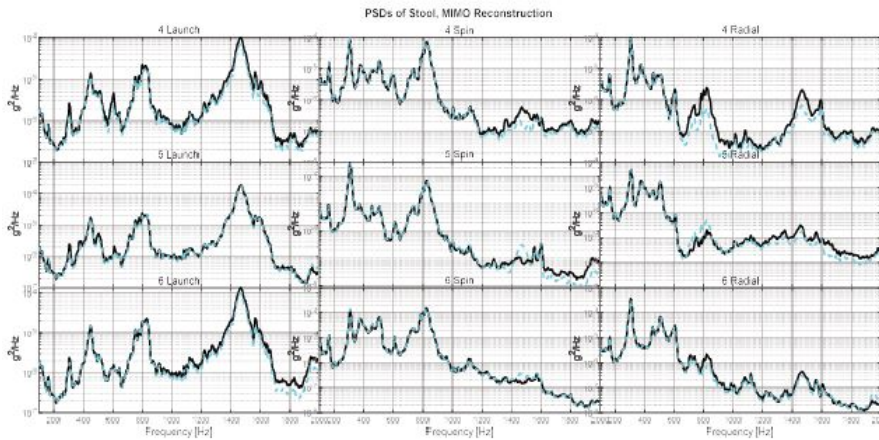


Figure 4.2: Original Flight Environment (Black) Compared to Environment Reconstructed Using First 9 FEM Modes (Cyan)

can also be used to understand the dynamic differences between flight and lab mode shapes, though it is not used here as flight mode shapes are not available. The lab mode shapes used in the following were obtained from the level 2 FEM. The free-free modes of the system were used, though fixed base modes have also been used for similar purposes [51, 52].

In the 100-2000 Hz frequency band, the level 2 FEM predicts three free-free elastic modes of the DUT in its lab configuration at 783, 785, and 885 Hz. The first and third of these are shown in Figure 4.1; the second mode is similar to the first mode but occurs in the out-of-page direction. When the 17 measured environment responses are projected onto the first 9 mode shapes (i.e., 6 rigid body modes and 3 elastic modes), the DUT environment is reconstructed with 3.1 dB error as shown in Figure 4.2. Therefore, the first 9 free-free FEM mode shapes roughly span the response space of the DUT’s in-flight motion up to 2000 Hz.

While the free-free modes of the DUT may not individually match its modes in flight, they span roughly the same physical response space as these in-flight modes up to 2000 Hz. In modal coordinates, the flight

[51] Mayes, *A Modal Craig-Bampton Substructure for Experiments, Analysis, Control and Specifications*, 2015.

[52] Harvie, “Using Modal Substructuring to Improve Shock & Vibration Qualification,” 2019.

environment can be written as,

$$[\mathbf{S}_{QQ}(\omega)] = [\mathbf{H}_{QF}(\omega)][\mathbf{S}_{FF}(\omega)][\mathbf{H}_{QF}(\omega)]^*, \quad (4.4)$$

where $[\mathbf{H}_{QF}(\omega)]$ is the FRF relating shaker forces to lab mode accelerations. In this study, the modal flight environment CPSD matrix $[\mathbf{S}_{QQ}(\omega)]$ is 9x9. The dimensions of $[\mathbf{H}_{QF}(\omega)]$ are the number of modal coordinates by the number of shakers. If there are fewer shakers than modal acceleration terms, the shaker forcing CPSD will be solved for in the least squares sense, and there will be error in reconstructing the modal environment. If the number of shakers and modes is the same, the FRF matrix is square, and a unique forcing CPSD can be solved for that will perfectly recreate the modal environment. In other words, one shaker can control a single modal response at each frequency line, so a modal environment with n modes can be perfectly reconstructed with n shakers.

Modal filtering can, therefore, be used to understand how well a flight environment can be reconstructed using a given lab test setup and how many shakers are required to do so. In this case, the environment can be reconstructed with 3.1 dB RMS error using 9 shakers. Often, fewer shakers are available, and each added shaker increases test cost, so it is advantageous to use fewer shakers when possible. In physical coordinates, shaker force is chosen to reconstruct the physical environment in the least squares sense, so when the number of shakers is reduced, error might increase significantly, and it is uncertain how this would affect stress simulated in the part. Since modes are independent, one could control to some desired modal responses while ignoring all others. Rather than recreating the physical response with least-squares error, if n shakers are available, the n most important modal responses can be reconstructed with no error.

The reduced modal environment is obtained by projecting the measured environment onto a set of modes that is expected to span the response space in the frequency band of interest and retaining the desired modal responses. The shaker force CPSD can be obtained by taking the pseudo-inverse of $[\mathbf{H}_{QF}(\omega)]$ in Eq. 4.4, which is obtained by multiplying the measured lab FRF $[\mathbf{H}_{XF}(\omega)]$ by the pseudo-inverse of the mode shape matrix,

$$[\mathbf{H}_{QF}(\omega)] = [\mathbf{\Phi}]^+[\mathbf{H}_{XF}(\omega)]. \quad (4.5)$$

In this test, the objective is to recreate stress in the DUT itself, so only the first three elastic modal responses are retained as suggested in [53]. The rigid body modes of the DUT do not produce any stress in the DUT. (However, it is worth noting that in practice the DUT may carry small electronic components or other appendages that are sensitive to the rigid body accelerations of the DUT. The discussion below assumes that this is not the case.) $[\mathbf{H}_{QF}(\omega)]$ was created using the same substructuring procedure, except only the two spin shakers and the radial shaker were attached to the DUT, and the DUT model included only the first three elastic modes. As seen in Figure 4.3, this simplified environment is

[53] Schoenherr *et al.*, "Using Modal Acceleration to Compare Two Environments of an Aerospace Component," 2023.

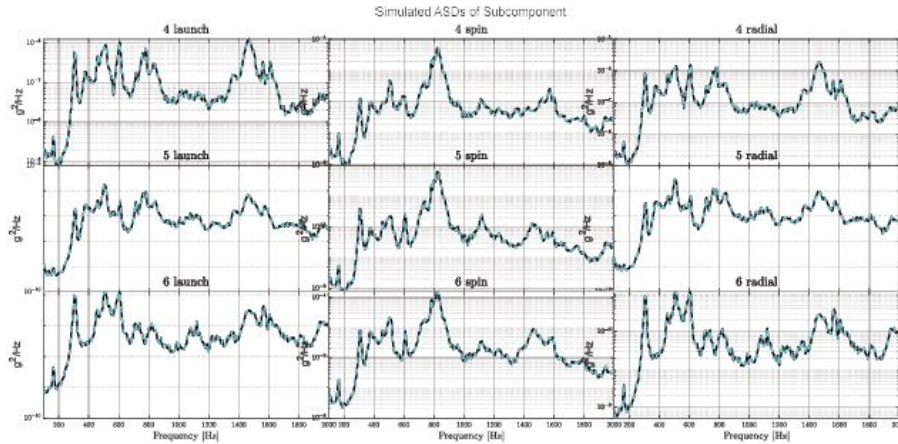


Figure 4.3: Elastic Environment (Black) and Simulated Reconstruction (Cyan) with Three Shakers

recreated perfectly using three shakers. While only radial and spin excitation are provided to the system, the modal filtered launch response is recreated accurately because the bending modes involve motion in the radial and launch directions, so the launch responses are correctly excited even though there are no shakers in the launch direction. The Shaker RMS voltages are also well within acceptable shaker limits, so this test could also be performed on the actual hardware.

Though modal responses are more directly correlated to in-flight stress than measured physical responses, there is some elastic motion in the flight environment that is not contained in the three elastic modal responses because they do not fully span the DUT's response space. This is evident in Fig. 4.2 as there are some frequencies where the original and filtered environment differ slightly. It is, therefore, important to select a set of lab mode shapes that recreates the flight environment with as little error as possible to minimize error in damage replication [53].

When attempting to replicate the environment in physical coordinates, there is least squares error as there are fewer shakers than accelerometer channels. In modal coordinates, the modal environment can be replicated perfectly as the number of shakers matches the number of lab modes, however, errors are observed when these modal responses are expanded to physical coordinates. To understand which of these errors is more significant, the modal acceleration PSDs obtained controlling to the modal filtered environment with three shakers are compared to those obtained controlling to the physical lab environment with 6 shakers in Figure 4.4. The modal responses are fairly similar in both tests, though they are underestimated at certain frequency lines in the six-shaker test. Visually, the most significant error occurs in recreating the first elastic modal response below 500 Hz, though the magnitude of this response is very small, so the damage recreated in the DUT is likely similar in both cases. Hence, using the modal projection procedure, stress in the DUT is conservatively simulated using half as many shakers as a normal test,

[53] Schoenherr *et al.*, "Using Modal Acceleration to Compare Two Environments of an Aerospace Component," 2023.

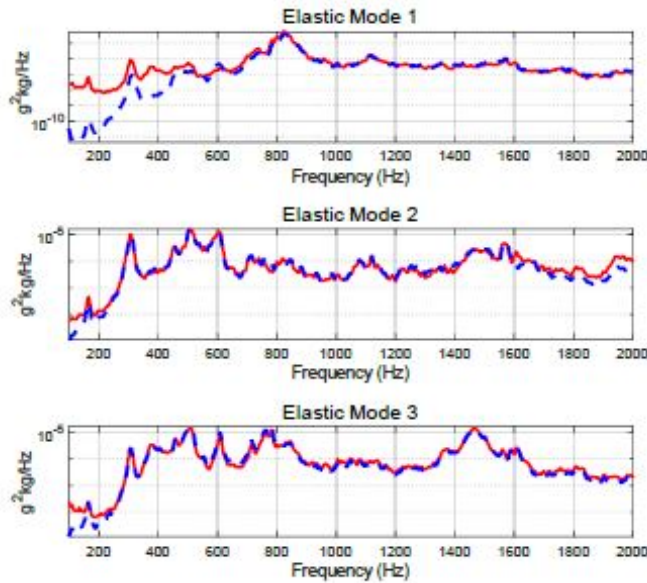


Figure 4.4: Lab Modal Responses in 3 Shaker Simplified Environment Test (Red) and 6 Shaker Unmodified Environment Test (Blue)

and the least squares errors in the two tests seem to have similar effects on the reconstructed elastic motion.

In summary, Modal filtering was used to understand the level of dynamic differences between the flight and lab setups. The first 9 free-free lab modes of the DUT were found to span the response space of the DUT in flight with little error up to 2000 Hz. The three elastic modal accelerations were retained and replicated with no error using three shakers, and this recreated elastic motion was similar to the elastic motion recreated using six shakers, attempting to control the 17 physical response channels. Therefore, modal filtering is useful in understanding how well a flight environment can be recreated given the lab setup's dynamics and for best utilizing shaker inputs when few are available.

Conclusion

In summary, this thesis provides the following contributions:

1. **Next Assembly Selection.** Tests were performed on a DUT that flew in a sounding rocket with varying levels of next assembly, and similar environment reconstruction was obtained on each. In doing so, a tradeoff between impedance, or how accurately the flight boundary condition is matched in the lab, and controllability, or how many shakers are required to control the lab setup's dynamics, was revealed. Including more of the next assembly improves the impedance match but makes the system harder to control as it has more active modes. Hence, with the number of shakers held constant at six, there was no noticeable difference in environment reconstruction across the lab configurations because of this tradeoff.
2. **Shaker Voltage Prediction.** The FRF Multiplication method was developed as a simpler alternative to dynamic substructuring for the purpose of coupling shaker and DUT dynamics. It only requires multiplying two FRF matrices, while frequency based substructuring requires drive point FRFs at DUT connection degrees of freedom, and component mode synthesis requires accurate knowledge of system mode shapes and is more mathematically complex. Hence, this procedure is useful in industry as it can reduce the time spent in the test planning process. FRF Multiplication was shown to be a great approximation of dynamic substructuring when the effective mass of the DUT at shaker degrees of freedom and the calibration mass are much higher than shaker armature masses and when the drive points are rigid. It was shown to be least accurate when these criteria were not met, when the shaker stinger mode occurred in the test frequency band, and when the stinger and DUT natural frequencies were close together.
3. **Number of Required Shakers.** The number of shakers to be used in a test was understood through a modal framework and is equal to the number of active modes of the lab test setup. When the number of shakers equals the number of active modes, then the only error in environment reconstruction will be due to the lab setup's dynamics not fully spanning those of the flight setup.

These contributions will allow multi-shaker tests to be planned more quickly and at a lower cost and will also help improve the accuracy of environment reconstruction in these tests, increasing certainty in the design process and allowing flight vehicle designs to be further optimized.

There are many unanswered questions in the field of environment testing that require future research. Some of these are listed below:

1. **Environment Estimation.** IMMATs require an increased number of control accelerometers relative to traditional single axis tests, and a flight environment must be defined at each of these accelerometers. In addition, it must be a physically meaningful flight environment - i.e., generic, enveloped specifications cannot be meaningfully employed in IMMATs. Hence, the flight environment must either be measured at an increased number of accelerometer locations, or it must be estimated at these locations. According to experts in the field, environments are sometimes estimated by applying some modeled forces to a finite element model of the full flight system and measuring the response on the DUT. While this is a useful practice, it is not generally known how accurate these estimated environments might be. Increased research in the area of environment estimation would, therefore, help establish an understanding of how to accurately estimate environments, and it would allow IMMATs to be performed more often due to the increased availability of environment data.
2. **Instrumentation Requirements.** On a similar note, it would be beneficial to understand how many accelerometers should be installed in flight, and where they should be placed. Ideally, the number of required accelerometers could be minimized, so understanding how few can be used to properly observe the DUT's motion would be very useful to companies. In addition, it would be useful to know if accelerometers are required on the DUT itself, or if accelerometers on the next assembly only are sufficient. For each test in this study that controlled the next assembly only, there was error in recreating the DUT's response, though it is uncertain given these results alone whether this is due to only having 6 shakers or whether it is due to failing to observe the DUT's motion fully. Understanding this would allow companies to optimize flight tests and to obtain the amount of data needed to reap the maximum benefit from an IMMAT.
3. **Testing Simplifications.** IMMATs typically involve an increased number of shakers, accelerometers, and a portion of the next assembly, though it may be difficult for companies to meet all of these requirements. The number of accelerometers might be limited by the availability of flight environment data. The next assembly might not be available to include in the test, or it might not be possible to remove a portion of it from the flight setup.

Enough modal shakers might not be available. Understanding the ideal number of shakers, accelerometers, and next assembly, as well as how significant error is expected to be when one of these criteria is not met, would allow companies to make reasonable compromises in the test design process to improve environment reconstruction while not incurring an unsustainable expense.

References

- [1] Rizzo, D. and Blackburn, M., “The History of a Decision: A Standard Vibration Test Method for Qualification,” *Journal of the IEST*, vol. 60, no. 1, January 2017, pp. 9–20. cited on p. 1
- [2] Skousen, T., Zwink, B., Reyes-Blanco, J., and Avitabile, P., “Actual Field Response Simulation Using Modified Laboratory Loading Conditions,” *Proceedings of the 41st International Modal Analysis Conference*, Austin, TX, February 2023. cited on p. 1
- [3] “Military Standard Environmental Test Methods for Aerospace and Ground Equipment,” MIL-STD-810, United States Air Force, June 1962. cited on p. 1
- [4] “Department of Defense Test Method Standard Environmental Engineering Considerations and Laboratory Tests,” MIL-STD-810G, Department of Defense, October 2008. cited on p. 1
- [5] Salter, J., “Problem Areas in Dynamic Testing,” *Proceedings of the Technical Meeting of the Institute of Environmental Sciences*, vol. 1963, 1963, pp. 49–54. cited on p. 1
- [6] Scharton, T. D., “Force Limited Vibration Testing Monograph,” RP-1403, NASA, 1997. cited on pp. 1, 2, 22
- [7] Barrett, R., “Techniques for Predicting Localized Vibratory Environments of Rocket Vehicles,” Technical Note D-1836, National Aeronautics and Space Administration, Huntsville, AL, October 1963. cited on p. 2
- [8] Klein, G. and Piersol, A., “The Development of Vibration Test Specifications for Spacecraft Applications,” Contractor Report CR-234, National Aeronautics and Space Administration, Los Angeles, CA, May 1965. cited on p. 2
- [9] Archer, J., “Structural Vibration Prediction,” SP-8050, National Aeronautics and Space Administration, June 1970. cited on p. 2
- [10] Hughes, T., *The Finite Element Method: Linear Static and Dynamic Finite Element Analysis*, 1st. Dover, 2000. cited on p. 2
- [11] O’Callahan, J., Avitabile, P., and Riemer, R., “System Equivalent Reduction Expansion Process,” *Proceedings of the 7th International Modal Analysis Conference*, Las Vegas, NV, 1989. cited on p. 2
- [12] Janssens, M. H. A., Verheij, J. W., and Loyau, T., “Experimental example of the pseudo-forces method used in characterisation of a structure-borne sound source,” *Applied Acoustics*, vol. 63, no. 1, January 2002, pp. 9–34. DOI: 10.1016/s0003-682x(01)00023-8 cited on p. 2

- [13] Mayes, R., Ankers, L., and Daborn, P., "Predicting System Response at Unmeasured Locations," *Experimental Techniques*, vol. 44, April 2020. DOI: 10.1007/s40799-020-00366-9 cited on p. 2
- [14] Chen, Y., Logan, P., Avitabile, P., and Dodson, J., "Non-Model Based Expansion from Limited Points to an Augmented Set of Points Using Chebyshev Polynomials," en, *Experimental Techniques*, vol. 43, no. 5, October 2019, pp. 521–543. DOI: 10.1007/s40799-018-00300-0 cited on p. 2
- [15] Taylor, C., Blough, J., DeClerck, J., VanKarsen, C., and Joshua, R., "A Comprehensive Review of Efforts to Improve Dynamic Environment Test Fixtures," *Proceedings of the 41st International Modal Analysis Conference*, Austin, TX, February 2023. cited on p. 2
- [16] Scharon, T. D., "Development of impedance simulation fixtures for spacecraft vibration tests," BBN-1703, NTRS Author Affiliations: Bolt, Beranek, and Newman, Inc. NTRS Document ID: 19690016937 NTRS Research Center: Legacy CDMS (CDMS), May 1969. cited on p. 2
- [17] Schoenherr, T., Clark, B., and Coffin, P., "Improve Replication of In-service Mechanical Environments." en, SAND2018-10187, 1493833, September 2018, SAND2018–10 187, 1 493 833. DOI: 10.2172/1493833 cited on pp. 2, 53
- [18] Rohe, D. P., Schultz, R. A., Schoenherr, T. F., and Skousen, T. J., "Comparison of Multi-Axis Testing of the BARC Structure with Varying Boundary Conditions," en, *Proceedings of the 37th International Modal Analysis Conference*, Orlando, FL, January 2019. cited on p. 2
- [19] Taylor, C., Blough, J., DeClerck, J., VanKarsen, C., and Joshua, R., "PDADyE Applied to a 2-attachment Fixture Case," *Proceedings of the 42nd International Modal Analysis Conference*, Orlando, FL, January 2024. cited on p. 2
- [20] Meyer, J., Joshua, R., Karve, P., Mahadevan, S., and Adams, D., "A Genetic Algorithm-Based Approach for Designing a Fixture that Preserves the Desired Dynamics of a Connecting Part," *Proceedings of the 42nd International Modal Analysis Conference*, Orlando, FL, January 2024. cited on p. 2
- [21] Whiteman, W. and Berman, M., "Fatigue Failure Results for Multi-Axial Versus Uniaxial Stress Screen Vibration Testing," *Shock and Vibration*, vol. 9, 2002, pp. 319–328. cited on p. 3
- [22] French, R., Handy, R., and Cooper, H., "A Comparison of Simultaneous and Sequential Single-Axis Durability Testing," *Experimental Techniques*, vol. 30, no. 5, October 2006, pp. 32–37. cited on p. 3
- [23] Gregory, D., Bitsie, F., and Smallwood, D., "Comparison of the Response of a Simple Structure to Single Axis and Multiple Axis Random Vibration Inputs," Sandia Report SAND2008-6945C, Sandia National Laboratories, Albuquerque, NM, 2008. cited on p. 3
- [24] Daborn, P., "Smarter dynamic testing of critical structures," eng, Accepted: 2014, Ph.D. University of Bristol, 2014. cited on pp. 3, 22

- [25] Mayes, R. and Rohe, D., "Physical Vibration Simulation of an Acoustic Environment with Six Shakers on an Industrial Structure," *Proceedings of the 34th International Modal Analysis Conference*, Orlando, FL, January 2016. cited on p. 3
- [26] Roberts, C. and Ewins, D., "Multi-axis vibration testing of an aerodynamically excited structure," *Journal of Vibration and Control*, vol. 24, no. 2, January 2018, pp. 427–437. DOI: 10.1177/1077546316642064 cited on p. 3
- [27] Schumann, C., Allen, M., Tuman, M., DeLima, W., and Dodgen, E., "Transmission Simulator Based MIMO Response Reconstruction," en, *Experimental Techniques*, vol. 46, no. 2, April 2022, pp. 287–297. DOI: 10.1007/s40799-021-00454-4 cited on pp. 3, 7, 10, 22, 47
- [28] Beale, C., Schultz, R., Smith, C., and Walsh, T., "Degree of Freedom Selection Approaches for MIMO Vibration Test Design," en, *Special Topics in Structural Dynamics & Experimental Techniques, Volume 5*, ser. Conference Proceedings of the Society for Experimental Mechanics Series, Cham: Springer International Publishing, 2023, pp. 81–90. DOI: 10.1007/978-3-031-05405-1_10 cited on p. 3
- [29] Khan, M. and Schoenherr, T., "Evaluating Degree of Freedom Selection Methods for MIMO Vibration Modeling," *Proceedings of the 42nd International Modal Analysis Conference*, Orlando, FL, January 2024. cited on p. 3
- [30] Rohe, D. P., Nelson, G. D., and Schultz, R. A., "Strategies for Shaker Placement for Impedance-Matched Multi-Axis Testing," en, *Sensors and Instrumentation, Aircraft/Aerospace, Energy Harvesting & Dynamic Environments Testing, Volume 7*, ser. Conference Proceedings of the Society for Experimental Mechanics Series, Cham: Springer International Publishing, 2020, pp. 195–212. DOI: 10.1007/978-3-030-12676-6_18 cited on pp. 3, 22, 46, 53, 67
- [31] Mayes, R., Ankers, L., Daborn, P., Moulder, T., and Ind, P., "Optimization of Shaker Locations for Multiple Shaker Environmental Testing," en, *Experimental Techniques*, vol. 44, no. 3, June 2020, pp. 283–297. DOI: 10.1007/s40799-019-00347-7 cited on pp. 3, 23, 30, 31
- [32] Hall, T., "Analytically Investigating Impedance-Matching Test Fixtures," en, *Sensors and Instrumentation, Aircraft/Aerospace, Energy Harvesting & Dynamic Environments Testing, Volume 7*, Walber, C., Walter, P., and Seidlitz, S., Eds., ser. Conference Proceedings of the Society for Experimental Mechanics Series, Cham: Springer International Publishing, 2020, pp. 21–31. DOI: 10.1007/978-3-030-12676-6_2 cited on p. 3
- [33] Tuman, M. J., Behling, M., Allen, M. S., DeLima, W. J., Hower, J., and Mayes, R. L., "Balancing Impedance and Controllability in Response Reconstruction with TS-IMMAT," en, *Experimental Techniques*, April 2023. DOI: 10.1007/s40799-023-00645-1 cited on p. 5
- [34] Tuman, M., Schumann, C., Allen, M., Delima, W., and Dodgen, E., "Investigation of Transmission Simulator-Based Response Reconstruction Accuracy," en, *Sensors and Instrumentation, Aircraft/Aerospace, Energy Harvesting & Dynamic Environments Testing, Volume 7*, ser. Conference Proceedings of the Society for Experimental Mechanics Series, Cham: cited on pp. 8–10

Springer International Publishing, 2022, pp. 65–76. DOI: 10.1007/978-3-030-75988-9_4

- [35] Behling, M., Thomason, B., Mayes, R., Allen, M., and DeLima, W., “A Simplified Method for Predicting Shaker Voltage in IMMATs,” *Submitted*, 2023. cited on p. 22
- [36] Paripovic, J. and Mayes, R. L., *Reproducing a Component Field Environment on a Six Degree-of-Freedom Shaker*, en, *Dynamic Substructures, Volume 4*, Series Title: Conference Proceedings of the Society for Experimental Mechanics Series, Cham: Springer International Publishing, 2021, pp. 73–78. DOI: 10.1007/978-3-030-47630-4_6 cited on p. 22
- [37] Schultz, R., “A Demonstration of Force Estimation and Regularization Methods for Multi-Shaker Testing,” en, *Sensors and Instrumentation, Aircraft/Aerospace, Energy Harvesting & Dynamic Environments Testing, Volume 7*, ser. Conference Proceedings of the Society for Experimental Mechanics Series, Cham: Springer International Publishing, 2020, pp. 229–243. DOI: 10.1007/978-3-030-12676-6_21 cited on p. 22
- [38] Schultz, R. and Avitabile, P., “Shape-constrained Input Estimation for Efficient Multi-shaker Vibration Testing,” en, *Experimental Techniques*, vol. 44, no. 4, August 2020, pp. 409–423. DOI: 10.1007/s40799-020-00361-0 cited on p. 22
- [39] Lang, G. and Snyder, D., “Understanding the Physics of Electrodynamical Shaker Performance,” *Sound and Vibration*, vol. 35, October 2001, pp. 24–33. cited on pp. 22, 31, 45
- [40] Fickenwirth, P., Schultze, J., Harvey, D., and Todd, M., “Shaker Capability Estimation Through Experimental Dynamic Substructuring,” *Proceedings of the 41st International Modal Analysis Conference*, Austin, Texas, February 2023. cited on pp. 23, 30
- [41] Schultz, R., “Vibration Test Design with Integrated Shaker Electro-Mechanical Models,” en, *Dynamic Substructures, Volume 4*, ser. Conference Proceedings of the Society for Experimental Mechanics Series, Cham: Springer International Publishing, 2021, pp. 63–72. DOI: 10.1007/978-3-030-47630-4_5 cited on pp. 23, 30
- [42] Hoffait, S., Marin, F., Simon, D., Peeters, B., and Golinval, J., “Virtual shaker testing at V2i: Measured-based shaker model and industrial test case,” en, *Proceedings of the 2016 International Conference on Noise and Vibration Engineering (ISMA)*, Leuven, Belgium, September 2016. cited on p. 27
- [43] Smallwood, D., “Characterizing Electrodynamical Shakers,” *Proceedings of the 43rd Institute of Environmental Sciences*, Los Angeles, CA, May 1997. cited on p. 27
- [44] Schultz, R., *Calibration of Shaker Electro-mechanical Models*, en, *Special Topics in Structural Dynamics & Experimental Techniques, Volume 5*, Series Title: Conference Proceedings of the Society for Experimental Mechanics Series, Cham: Springer International Publishing, 2021, pp. 133–144. DOI: 10.1007/978-3-030-47709-7_12 cited on pp. 27, 28, 30, 49

- [45] Dal Borgo, M., Ghandchi Tehrani, M., and Elliott, S. J., "Identification and analysis of nonlinear dynamics of inertial actuators," en, *Mechanical Systems and Signal Processing*, vol. 115, January 2019, pp. 338–360. DOI: 10.1016/j.ymssp.2018.05.044 cited on p. 29
- [46] Klerk, D., Rixen, D., and Voormeeren, S., "General Framework for Dynamic Substructuring: History, Review, and Classification of Techniques," *Aiaa Journal - AIAA J*, vol. 46, May 2008, pp. 1169–1181. DOI: 10.2514/1.33274 cited on p. 32
- [47] Rao, S. S., *Mechanical vibrations*, eng, 5th ed. Upper Saddle River: Prentice Hall, 2011, OCLC: 804737767. cited on p. 40
- [48] Taylor, C., "Using Transfer Path Analysis and Frequency Based Substructuring To Develop A Robust Vibration Laboratory Dynamic Test Fixture Design Process," en, Master of Science in Mechanical Engineering, Michigan Technological University, Houghton, Michigan, 2020. DOI: 10.37099/mtu.dc.etr/1097 cited on p. 42
- [49] Schoenherr, T., Coffin, P., and Clark, B., *Use of Topology Optimization to Design Shock and Vibration Test Fixtures*, en, *Sensors and Instrumentation, Aircraft/Aerospace, Energy Harvesting & Dynamic Environments Testing, Volume 7*, Walber, C., Walter, P., and Seidlitz, S., Eds., Series Title: Conference Proceedings of the Society for Experimental Mechanics Series, Cham: Springer International Publishing, 2020, pp. 77–92. DOI: 10.1007/978-3-030-12676-6_8 cited on p. 42
- [50] Behling, M., Thomason, B., Mayes, R., Allen, M., DeLima, W., and Hower, J., "Improving IMMAT Planning Through Shaker Modeling and Modal Filtering," *Proceedings of the 42nd International Modal Analysis Conference*, Orlando, FL, January 2024. cited on p. 53
- [51] Mayes, R., *A Modal Craig-Bampton Substructure for Experiments, Analysis, Control and Specifications*, en, *Dynamics of Coupled Structures, Volume 4*, Series Title: Conference Proceedings of the Society for Experimental Mechanics Series, Cham: Springer International Publishing, 2015, pp. 93–98. DOI: 10.1007/978-3-319-15209-7_9 cited on p. 54
- [52] Harvie, J., "Using Modal Substructuring to Improve Shock & Vibration Qualification," en, *Topics in Modal Analysis & Testing, Volume 9*, ser. Conference Proceedings of the Society for Experimental Mechanics Series, Cham: Springer International Publishing, 2019, pp. 227–239. DOI: 10.1007/978-3-319-74700-2_24 cited on p. 54
- [53] Schoenherr, T. and Khan, M., "Using Modal Acceleration to Compare Two Environments of an Aerospace Component," Austin, TX, February 2023. cited on pp. 55, 56

Appendices



Shaker Selection Algorithm

Prior to performing any test, it is helpful to have a means of ensuring that the shaker locations used are adequate. The theory just presented shows how the spectra obtained in a MIMO test are related to the FRFs of the system of interest. Those FRFs can be created from a finite element model or measured experimentally; in this work we take the latter approach as detailed later.

The iterative shaker placement algorithm from [30] was adapted to find the shakers locations used in this work. First, the average dB difference of two ASDs for all relevant accelerometer channels at a frequency line is computed using Eq. (14). After computing an error value for each frequency line, a final metric is computed using Eq. (15). This final error number represents the average dB error across all accelerometers and frequency line. A low error metric communicates a successful reconstruction test and will be used moving forward to compare various tests. With the error metric defined, the shaker location algorithm used in this work is as follows:

[30] Rohe *et al.*, "Strategies for Shaker Placement for Impedance-Matched Multi-Axis Testing," 2020.

1. Start with a pool of all possible forcing input locations from the roving hammer test of the component
2. Simulate the MIMO response for each forcing input location in the remaining pool (controlling to the eight plate accelerometers)
3. Identify the forcing input location that produces the lowest error on the controlled DOF (plate accelerometers). Add that input location to the set of chosen forcing locations and remove from the pool of possible locations.
4. Repeat steps 2-4 with the kept forcing input location/s from the previous iterations plus each candidate location and again keep the best candidate location until the number of desired shakers is reached.

The optimization was terminated once it determined the six best shaker locations. The error metric in Eq. (15) was also used in the results that follow to provide a measure of how successful a particular test was in recreating the desired environment.

B

Shaker Parameter Sensitivity Study

The following figures show the effects that varying the unknown shaker parameters has on the acceleration / voltage FRF from the shaker model.

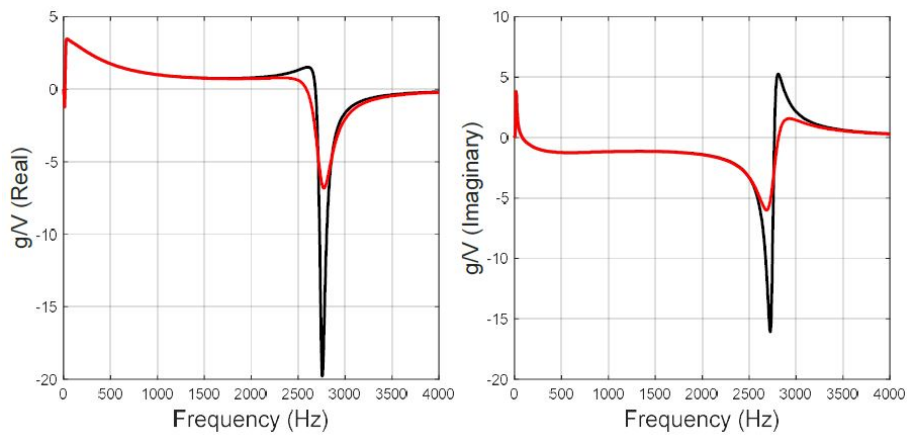


Figure B.1: Analytical Acceleration/Voltage FRF with Nominal Stinger Damping Value (Black) and 3x Nominal Value (Red)

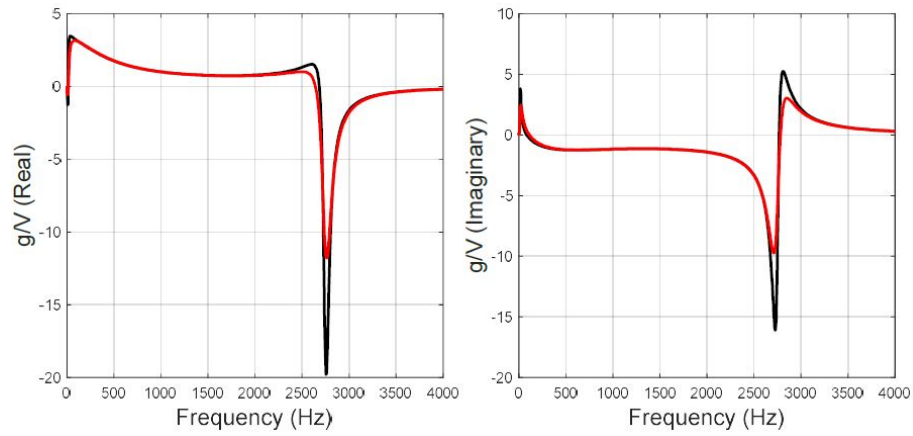


Figure B.2: Analytical Acceleration/Voltage FRF with Nominal Flexure Damping Value (Black) and 50x Nominal Value (Red)

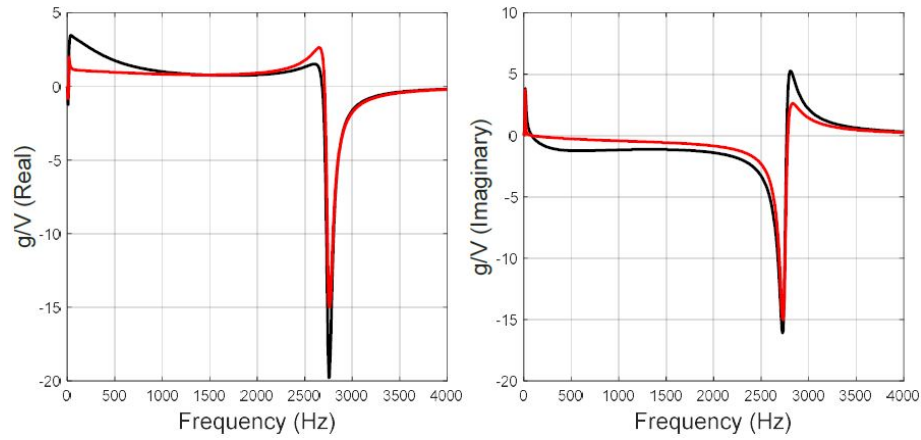


Figure B.3: Analytical Acceleration/Voltage FRF with Nominal Resistance Value (Black) and 3x Nominal Value (Red)

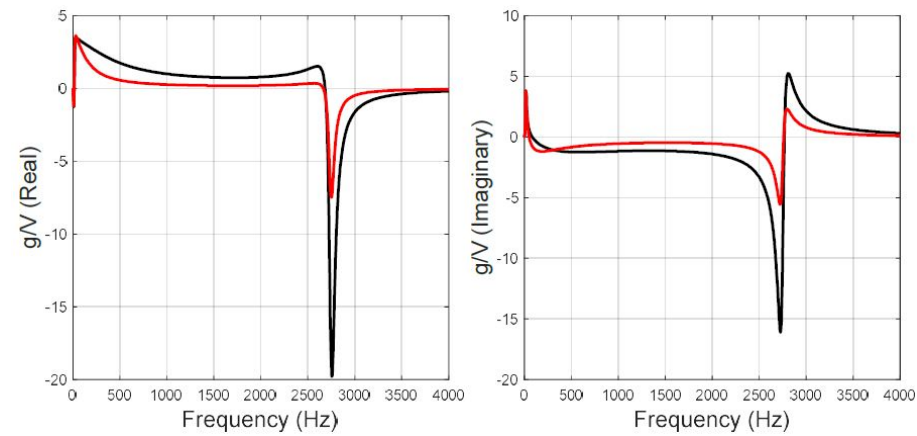


Figure B.4: Analytical Acceleration/Voltage FRF with Nominal Inductance Value (Black) and 3x Nominal Value (Red)

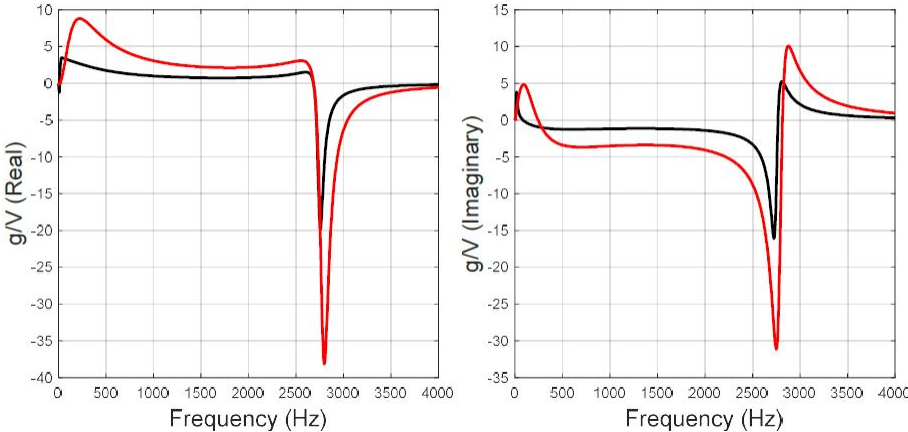


Figure B.5: Analytical Acceleration/Voltage FRF with Nominal Back-EMF Constant (Black) and 3x Nominal Value (Red)